

1        **Ca-looping for postcombustion CO<sub>2</sub> capture: A comparative**  
2        **analysis on the performances of dolomite and limestone**

3                    J. M. Valverde<sup>a\*</sup>, P. E. Sanchez-Jimenez<sup>b</sup>, L. A. Perez-Maqueda<sup>b</sup>

4        <sup>a</sup> Faculty of Physics. University of Seville. Avenida Reina Mercedes s/n, 41012 Sevilla, Spain

5                    <sup>b</sup> Instituto de Ciencia de Materiales de Sevilla (C.S.I.C.-Univ.

6                    Seville), Americo Vespucio 49, 41092 Sevilla, Spain

7                    \* **Corresponding author:** Phone no. +34 954550960.

8                    Fax no. +34 954239434. Email: jmillan@us.es

9        **Keywords:** CO<sub>2</sub> capture; Calcium looping; limestone; dolomite

## Abstract

The low cost and wide availability of natural limestone ( $\text{CaCO}_3$ ) is at the basis of the industrial competitiveness of the Ca-looping (CaL) technology for postcombustion  $\text{CO}_2$  capture as already demonstrated by  $\sim 1 \text{ Mw}_t$  scale pilot projects. A major focus of studies oriented towards further improving the efficiency of the CaL technology is how to prevent the gradual loss of capture capacity of limestone derived CaO as the number of carbonation/calcination cycles is increased. Natural dolomite ( $\text{MgCa}(\text{CO}_3)_2$ ) has been proposed as an alternative sorbent precursor to limestone. Yet, carbonation of MgO is not thermodynamically favorable at CaL conditions, which may hinder the capture performance of dolomite. In the work described in this paper we carried out a thermogravimetric analysis on the multicyclic capture performance of natural dolomite under realistic regeneration conditions necessarily implying high calcination temperature, high  $\text{CO}_2$  concentration and fast transitions between the carbonation and calcination stages. Our study demonstrates that the sorbent derived from dolomite has a greater capture capacity as compared to limestone. SEM analysis shows that MgO grains in the decomposed dolomite are resistant to sintering under severe calcination conditions and segregate from CaO acting as a thermally stable support which mitigates the multicyclic loss of CaO conversion. Furthermore, full decomposition of dolomite is achieved at significantly lower calcination temperatures as compared to limestone, which would help improving further the industrial competitiveness of the technology.

## 29 I. INTRODUCTION

30 The Ca-looping (CaL) technology has recently emerged as a potentially feasible process  
31 for postcombustion CO<sub>2</sub> capture [1–3]. As a main advantage over other technologies it  
32 stands the low cost, wide availability and harmlessness towards the environment of natu-  
33 ral limestone to be used as CaO precursor for CO<sub>2</sub> capture [4, 5]. In this process, CO<sub>2</sub> is  
34 chemisorbed on the surface of CaO particles fluidized in a gas-solid reactor (carbonator)  
35 by the postcombustion gas stream at atmospheric pressure and temperatures about 650°C.  
36 The solids partially carbonated after typically short residence times (of a few minutes) are  
37 circulated into a second gas-solid reactor (calciner) where CaO is regenerated by calcina-  
38 tion at atmospheric pressure and a gas stream of highly concentrated CO<sub>2</sub> is retrieved for  
39 compression and storage.

40 The CaL technology is being demonstrated in large-scale pilot plants (up to 1.7 MW<sub>t</sub>)  
41 showing efficient and sustainable CO<sub>2</sub> capture [3, 6]. A typical run commences by precalcini-  
42 ng the initial inventory of limestone in air after which the calciner is set to oxy-combustion  
43 mode and the circulation of solids in the loop is started. Burning fuel with pure oxygen  
44 (oxy-combustion) ensures a high CO<sub>2</sub> concentration in the gas exiting the calciner and a  
45 sufficiently high temperature (close to 950°C) to achieve complete CaO regeneration in short  
46 residence times [3, 6–10]. However, oxy-combustion imposes an energy penalty (due to the  
47 consumption of fuel and oxygen) and generates additional CO<sub>2</sub> [8, 11–13]. Moreover, the  
48 carbonation activity of CaO regenerated at high temperature and under high CO<sub>2</sub> con-  
49 centration suffers a marked drop, which is particularly intense in the first cycles [10, 14].  
50 Other causes of decay of the sorbent capture capacity are irreversible sulphation due to SO<sub>2</sub>  
51 (present in the flue gas and produced in the calciner by oxy-combustion) and losses of fine

52 particles generated by attrition [3, 15]. It is thus necessary to feed the calciner periodically  
53 with a makeup flow of fresh limestone to compensate for sorbent deactivation. As opposed  
54 to the sorbent derived from calcination of the initial limestone inventory, CaO derived from  
55 the makeup flow is obtained by calcination in a high CO<sub>2</sub> partial pressure environment.

56 Another naturally occurring mineral that can be used as CaO precursor is dolomite  
57 (CaMg(CO<sub>3</sub>)<sub>2</sub>), which is also abundantly available at low price [1, 16, 17]. Arguably, the  
58 irreversible decomposition of MgCO<sub>3</sub> would enhance the surface area of the calcined sorbent  
59 [18], which should favor the CaO reactivity in the fast phase controlled by carbonation on  
60 the surface of the solids. Moreover, the presence of MgO in calcined dolomite is expected  
61 to increase the thermal stability of the sorbent and help mitigating the loss of CaO carbon-  
62 ation reactivity, which is generally attributed to its superior resistance to sintering at high  
63 calcination temperatures. The ultimate mechanism governing the thermal decomposition of  
64 dolomite is however not well understood yet [19–21]. The Tamman temperature indicating  
65 the initiation of sintering of MgO ( $T_t \simeq 1276^\circ\text{C}$ ) [16] is only slightly above the Tamman  
66 temperature of CaO ( $T_t \simeq 1170^\circ\text{C}$ ) [16] being both values well over the typical calcina-  
67 tion temperatures at CaL conditions. Thus, it is unclear why MgO should be resistant to  
68 sintering while CaO is not. Furthermore, carbonation of MgO is not thermodynamically  
69 favorable at CaL conditions [1, 22]. Hence, the stoichiometric CO<sub>2</sub> capture capacity (ratio  
70 of mass of CO<sub>2</sub> chemisorbed to mass of CaO·MgO) of calcined dolomite at CaL conditions  
71 is just 0.46 as compared to 0.79 for calcined limestone. Experimental results show accord-  
72 ingly that the capture capacity of dolomite stays well below that of limestone after a certain  
73 number of carbonation/calcination cycles [1] even though it must be remarked that most  
74 lab-scale tests on dolomite or CaO·MgO synthetic composites do not mimic realistic CaL  
75 conditions for postcombustion capture [23–26]. For example, Albrecht et al. [24] observed

76 that the presence of inert MgO served to increase the conversion of CaO after a very large  
77 number of carbonation/calcination cycles (up to 1250). However, these cycles were con-  
78 ducted isothermally at 750°C, subjecting the sample to a 25% CO<sub>2</sub>/75% N<sub>2</sub> gas mixture  
79 for carbonation during 20 min and calcining it under N<sub>2</sub> during 30 min. A first attempt to  
80 compare the multicyclic capture performances of dolomite and limestone when subjected to  
81 severe calcination conditions (940°C, 70% vol CO<sub>2</sub>) has been recently made [27] by means  
82 of a lab-scale bubbling fluidized bed (gas velocities of about 0.5 m/s). Results showed that,  
83 despite of its lower Ca content, the sorbent derived from dolomite had a greater capture  
84 capacity than limestone derived CaO. However, the sorbents were subjected in this study to  
85 only 5 calcination/carbonation cycles in which carbonation was prolonged up to completion  
86 and the materials were cooled down to ambient temperature between stages, which is not  
87 representative of realistic CaL conditions.

88 Realistic CaL conditions for postcombustion capture necessarily involve short residence  
89 times (of just a few minutes), low CO<sub>2</sub> concentration (about 15% vol) for partial carbonation  
90 at around 650°C, high temperature (above 900°C) and high CO<sub>2</sub> concentration (above 70%  
91 vol) in the calciner for sorbent regeneration and precalcination of the makeup flow of solids,  
92 and very fast transitions between the carbonation and calcination stages (typically of a  
93 few seconds) [15, 28]. Moreover, the dual fluidized bed in practice would be operated by  
94 rapid gas flows (gas velocities in the range 5 - 10 m/s) in the fast fluidization regime [29]  
95 characterized by a high mass/heat transfer efficiency, which is likely impaired in bubbling  
96 beds (operated at small gas velocities) wherein gas-solids contacting effectiveness is hindered  
97 by the development of gas bubbles [7, 30]. Mass/heat transfer inefficiency may be avoided  
98 by means of TGA tests, which however usually fail to reproduce simultaneously the rapid  
99 transitions between stages and high CO<sub>2</sub> partial pressure in the calcination environment.

100 According to process simulations [2, 11, 31, 32] the efficiency of the CaL technology is  
101 extraordinarily dependent upon the sorbent capture performance. Thus, it is of paramount  
102 importance to characterize it at realistic conditions in order to extract from simulations  
103 useful information for the optimum design and operational parameters to scale-up the tech-  
104 nology. In the present manuscript we show a comparative study on the multicyclic CO<sub>2</sub>  
105 capture behavior of natural dolomite and limestone by means of thermogravimetric analysis  
106 (TGA) tests carried out at conditions closely resembling those to be expected in postcombus-  
107 tion capture applications. The role of precalcination conditions and the effect of introducing  
108 a recarbonation stage between carbonation and calcination stages will be a particular focus  
109 of our study. The incorporation of a recarbonator reactor to the CaL process is thought  
110 to improve its efficiency by minimizing the required makeup flow of fresh limestone and  
111 the heat demand in the calciner [33–35] albeit in previously reported TGA tests demon-  
112 strating the beneficial effect of recarbonation [33, 35, 36] the sorbent was regenerated by  
113 calcination in air. More recent works have evidenced that the capture capacity of CaO  
114 derived by precalcination of limestone in air and subsequently regenerated by calcination  
115 at high temperature/high CO<sub>2</sub> concentration is actually hampered by the introduction of a  
116 recarbonation stage [14, 37], which shed doubts on the usefulness of incorporating into the  
117 technology an additional recarbonator reactor. As will be seen in this manuscript dolomite  
118 and limestone respond in a very distinct way to recarbonation as a function of precalcination  
119 conditions. Scanning Electron microscopy (SEM) analysis will be used in our study to gain  
120 fundamental knowledge on the mechanisms governing the behavior of both natural CaO  
121 precursors.

## 122 II. MATERIALS AND METHODS

123 The materials employed in our work are natural limestone of high purity (99.62%  $\text{CaCO}_3$ ,  
124  $\text{SiO}_2 < 0.05\%$ ,  $\text{Al}_2\text{O}_3 < 0.05\%$ , 0.24%  $\text{MgO}$ , 0.08%  $\text{Na}_2\text{O}$ ) as received from Matagallar quarry  
125 (Pedrera, Spain) and a purified natural dolomite ( $\text{MgCa}(\text{CO}_3)_2$ ) purchased from Alfa Aesar  
126 (CAS: 12001-27-3). X-ray diffraction (XRD) patterns measured in our work are shown in  
127 Fig. 1. As may be seen, both samples are characterized by a high purity with only a minor  
128 presence of  $\text{CaCO}_3$  impurities in dolomite (as revealed by the small diffraction peak located  
129 in the major calcite peak at  $2\theta \approx 29.2^\circ$ ).

130 The multicyclic  $\text{CO}_2$  capture behavior of limestone and dolomite samples has been ana-  
131 lyzed by means of carbonation/calcination and carbonation/recarbonation/calcination cy-  
132 cles carried out using a Q5000IR TG analyzer (TA Instruments). This instrument is  
133 equipped with a furnace heated by infrared halogen lamps and a high sensitivity balance  
134 ( $< 0.1 \mu\text{g}$ ) with a minimum baseline dynamic drift ( $< 10 \mu\text{g}$ ). Infrared heating allows fast  
135 and controlled heating/cooling rates ( $300^\circ\text{C}/\text{min}$ ) with rather small fluctuations ( $< \pm 4^\circ\text{C}$ ).  
136 In this way, the transition between the carbonation and calcination stages may be shortened  
137 to tens of seconds in contrast with typical TGA tests carried out by using common furnaces  
138 with low heating rates (usually below  $25^\circ\text{C}/\text{min}$ ). This is a relevant issue when the sor-  
139 bent is regenerated under high  $\text{CO}_2$  partial pressure since during slow heating it will suffer  
140 appreciable recarbonation until the temperature reaches a sufficiently high value (close to  
141  $900^\circ\text{C}$ ) to reverse the reaction towards decarbonation, which seriously affects its capture  
142 performance [14].

143 Carbonation/calcination (carb/cal) cycles in our TGA tests consisted of 5 min carbona-  
144 tion at  $650^\circ\text{C}$  (85% air/15%  $\text{CO}_2$  vol/vol) and 5 min calcination at  $950^\circ\text{C}$  (70%  $\text{CO}_2$ /30% air

145 vol/vol). For comparison, carb/cal tests were also carried out in which calcination was per-  
146 formed at 925°C and 900°C under 70% CO<sub>2</sub>/30% air vol/vol, and at 850°C in air. In regards  
147 to carbonation/recarbonation/calcination (carb/recarb/cal) cycles, a 3 min recarbonation  
148 stage at 800°C (10% air/90% CO<sub>2</sub> vol/vol) was introduced in between the carbonation and  
149 calcination stages. TGA tests were initiated by subjecting the samples to different pre-  
150 calcination programs in-situ. On one hand, precalcination was carried out by heating the  
151 samples in air at a slow rate (20°C/min) up to 850°C with the goal of replicating the pre-  
152 calcination conditions of the initial solids inventory in the practical application. On the  
153 other hand, precalcination was performed by heating up the samples under high CO<sub>2</sub> par-  
154 tial pressure (70% CO<sub>2</sub>/30% air vol/vol) up to 950°C (925°C and 900°C in some tests) at  
155 a fast rate (300°C/min), which was intended to mimic precalcination of the makeup flow  
156 of solids periodically fed into the calciner at practice (due to technical limitations the heat-  
157 ing rate was set to 20°C/min from ambient temperature up to 450°C, which is below the  
158 reported decomposition temperatures for both materials [23]). The gas flow rate in all the  
159 tests was kept small enough (100 cm<sup>3</sup>min<sup>-1</sup>) as to neglect external mass transfer effects. A  
160 fixed sample mass of 10 mg was employed in all the runs, which allows dismissing also any  
161 effect of diffusion resistance through the sample on the reaction rate [38]. Particle size in  
162 our samples was below 500 μm, thus intra-particle diffusion resistance can be disregarded  
163 too [39, 40]. TGA tests were complemented with microscopy analysis of the cycled samples  
164 by means of a ultra high-resolution Scanning Electron Microscope (SEM HITACHI S5200).



### 165 III. EXPERIMENTAL RESULTS AND DISCUSSION

#### 166 A. CO<sub>2</sub> capture capacity

167 In order to take into account the presence of inert MgO in the sorbent derived from  
168 dolomite, the appropriate parameter for practical purposes to characterize the sorbent per-  
169 formance is the capture capacity, which is defined as the ratio of mass of CO<sub>2</sub> captured to  
170 the mass of sorbent before each carbonation stage (including both CaO and MgO in the  
171 case of dolomite). Figure 2 shows multicyclic capture capacity results from carb/cal tests in  
172 which dolomite and limestone samples were precalcined in air and regenerated either in air at  
173 850°C (Fig. 2a) or under 70%CO<sub>2</sub> at 950°C (Fig. 2b), respectively. As might be expected,  
174 dolomite exhibits a lower capture capacity during the first cycles after precalcination in air  
175 but it deactivates with the cycle number at a lower rate as compared with limestone. Under  
176 these conditions (sorbent regeneration in air, Fig. 2a) limestone deactivation is not marked  
177 and both sorbents exhibit a similar performance after the 5th carb/cal cycle. However, the  
178 scenario is radically changed when the sorbents are regenerated under realistic (postcom-  
179 bustion capture) calcination conditions (Fig. 2b). In this case, limestone suffers a drastic  
180 drop of its capture capacity after regeneration and it falls below 0.05 in just 10 cycles. In  
181 contrast, dolomite deactivates at a much lower rate. As a result, the capture capacity of  
182 dolomite is twice that of limestone after 20 cycles.

183 The effect of recarbonation on the performance of both sorbents precalcined in air and  
184 regenerated under high CO<sub>2</sub> concentration is illustrated by Figs. 3a and 3b. As can be  
185 seen, recarbonation is actually detrimental for the carbonation activity of limestone cycled  
186 under these conditions. Conversely, recarbonation does not cause an appreciable effect on  
187 the performance of dolomite. Likewise, the behavior of dolomite is not essentially changed

188 by the conditions of precalcination as seen in Fig. 4 where capture capacity data are plotted  
189 from carb/calc tests in which precalcination was carried out either in air at 850°C or under  
190 70%CO<sub>2</sub> at 950°C. Contrarily, precalcination conditions play a relevant role on the multi-  
191 cyclic behavior of limestone (see Fig. 4). Severe precalcination conditions cause a significant  
192 drop of the capture capacity of limestone derived CaO in the 1st cycle but it serves to miti-  
193 gate its progressive decay with the number of cycles. After 20 cycles, the capture capacity of  
194 the limestone sample precalcined under high CO<sub>2</sub> concentration is about 0.08 as compared  
195 to just 0.04 when limestone was precalcined in air. Still dolomite exhibits a neatly higher  
196 capture capacity also when precalcination conditions are severe (see Fig. 5). Figure 6 shows  
197 the effect of recarbonation on the performance of the sorbents precalcined and regenerated  
198 under severe conditions. Interestingly, recarbonation has in this case a favorable influence on  
199 the performance of limestone whereas the behavior of dolomite remains quite insensitive to  
200 recarbonation up to the 10th cycle after which the capture capacity of the sorbent subjected  
201 to recarbonation becomes only slightly hindered.

202 As a summary, TGA results demonstrate that dolomite exhibits a multicyclic capture  
203 capacity which does not suffer remarkable variations with either sorbent recarbonation or  
204 the conditions of precalcination. Conversely, the behavior of limestone is highly dependent  
205 on both. Only if limestone is precalcined under severe conditions involving high CO<sub>2</sub> concen-  
206 tration (similar to those of regeneration) and is subjected to an intermediate recarbonation  
207 stage, its capture capacity may keep the pace with that of dolomite subjected to ordinary  
208 carb/calc cycles as seen in Fig. 7. From the point of view of sorbent capture performance  
209 at realistic CaL conditions, these results suggest that the use of natural dolomite for post-  
210 combustion capture would yield an efficiency improvement of the CaL technology, which is  
211 comparable to that of introducing a recarbonator reactor when using limestone (with the

212 added requirement, if limestone is employed, of precalcining under high  $\text{CO}_2$  partial pressure  
213 instead of air in order to avoid marked deactivation as seen in our work). An additional  
214 gain of efficiency may be achieved by the possibility of calcining at lower temperatures. This  
215 relevant issue will be discussed in detail in section IV. In regards to the sorbent behavior, it  
216 is interesting to remark that the capture capacity of dolomite is practically insensitive to the  
217 temperature of precalcination/regeneration in the range of temperatures between  $900^\circ\text{C}$  and  
218  $950^\circ\text{C}$  as seen in Fig. 7, which stresses further the main role of  $\text{MgO}$  on avoiding sintering  
219 and deactivation of  $\text{CaO}$  at high temperatures.

## 220 B. CaO conversion

221 Let us recall that, for practical purposes, the parameter used above to compare the mul-  
222 ticyclic  $\text{CO}_2$  capture performances of dolomite and limestone has been the capture capacity.  
223 From a fundamental perspective it is also interesting to look at the  $\text{CaO}$  conversion defined  
224 as the ratio of mass of  $\text{CaO}$  converted in each carbonation stage to the mass of  $\text{CaO}$  initially  
225 present in the sorbent after calcination. In the case of limestone,  $\text{CaO}$  conversion is readily  
226 obtained multiplying the capture capacity by the factor  $M_{\text{CaO}}/M_{\text{CO}_2}$  where  $M_{\text{CaO}} = 56$   
227  $\text{g/mol}$  and  $M_{\text{CO}_2} = 44 \text{ g/mol}$  are the molecular weights of  $\text{CaO}$  and  $\text{CO}_2$ , respectively.  
228 For dolomite, the sorbent derived after calcination consists of  $\text{MgO}\cdot\text{CaO}$ .  $\text{CaO}$  conversion is  
229 then obtained multiplying the capture capacity by the factor  $(1 + M_{\text{MgO}}/M_{\text{CaO}})M_{\text{CaO}}/M_{\text{CO}_2}$   
230 where  $M_{\text{MgO}} = 40 \text{ g/mol}$  is the molecular weight of  $\text{MgO}$ . Figure 8 shows data on multicyclic  
231  $\text{CaO}$  conversion for both sorbents precalcined either in air (at  $850^\circ\text{C}$ ) or under  $70\%\text{CO}_2$  (at  
232  $950^\circ\text{C}$ ) and regenerated under severe conditions (note the log-log scale). Multicyclic  $\text{CaO}$   
233 conversion data reported in the literature is usually fitted by the semi-empirical equation  
234 [41–43]

$$X_N = X_r + \frac{X_1}{k(N-1) + (1 - X_r/X_1)^{-1}}; \quad (N = 1, 2, \dots) \quad (1)$$

235 where  $N$  is the cycle number,  $X_1$  is CaO conversion at the 1st cycle,  $k$  is a deactivation  
 236 constant and  $X_r$  is the so-called residual conversion, which is asymptotically approached  
 237 for a very large number of cycles. Most of TGA data obtained for natural limestones can  
 238 be reasonably well fitted using Eq. 1 with a residual conversion between 0.07 and 0.08 and  
 239 a deactivation constant  $k$  around 0.5 [41, 44]. Usually, process simulations and economic  
 240 analysis on the CaL technology rely on these values to characterize the sorbent behavior  
 241 [2, 12, 31, 33, 34, 45]. Yet, most lab-scale tests are not carried out under realistic (post-  
 242 combustion capture) calcination conditions due to technical limitations as explained above.  
 243 As may be seen in Fig. 8, CaO conversion data obtained in our work for limestone precal-  
 244 cined and regenerated under high CO<sub>2</sub> concentration still converges towards a residual value  
 245 ( $X_r = 0.079$ ), which fits within the interval commonly reported for limestones precalcined  
 246 and regenerated under low CO<sub>2</sub> concentration even though the deactivation constant ob-  
 247 tained from our data is substantially higher ( $k = 0.85$ ). In regards to the multicyclic CaO  
 248 conversion of limestone precalcined in air and regenerated under high CO<sub>2</sub> concentration, in  
 249 the first 10 cycles it follows a trend marked by a drastic drop which cannot be satisfactorily  
 250 fitted by Eq. 1 (see Fig. 8). Under these conditions, Eq. 1 conforms well to the evolution of  
 251 CaO conversion data only from the 10th cycle yielding a residual value of just  $X_r = 0.034$ .  
 252 On the other hand, the behavior of CaO conversion for dolomite does not exhibit such a  
 253 critical dependence on precalcination conditions and reaches a quite high residual value as  
 254 compared to limestone. Note that, even after precalcination under severe conditions, CaO  
 255 conversion for dolomite in the 1st cycle is about  $X_1 = 0.794$  whereas for limestone it falls  
 256 down to just  $X_1 = 0.476$

Our TGA results indicate that the CaO skeleton derived from precalcining limestone in air is highly reactive, yet when the sorbent is regenerated under high CO<sub>2</sub> concentration/high temperature (a must for postcombustion capture) it suffers a drastic deactivation which is additionally intensified by recarbonation. SEM pictures of limestone and dolomite samples precalcined in air and subjected to carb/calc cycles under severe regeneration conditions are shown in Fig. 9. Clearly, limestone derived CaO appears as markedly sintered. The consequent reduction of its reactive surface area is in accordance with the significant drop of the fast carbonation activity obtained from the TGA tests (Fig. 4a). On the other hand, the cycled dolomite sample exhibits a much higher porosity. As inferred from TEM (in-situ) and XRD analysis reported elsewhere [21] on dolomite crystals calcined at temperatures in the range 500–1000°C, decomposition of dolomite occurs by de-mixing of a metastable CaO·MgO precursor and the subsequent formation of pure CaO and MgO crystals via oriented aggregation and sintering, which is favored by high ion diffusivity, although it must be noticed that calcination in those tests was carried out in air and vacuum (we will come back to this argument in section IV). In our SEM pictures, individual MgO grains segregated from sintered CaO can be clearly identified (Fig. 9). MgO grains have a regular size of around 100nm and appear to be rather resistant to sintering. In fact, these SEM images of cycled dolomite samples show a striking resemblance with SEM images shown in our previous work [46] of a CaO-based sorbent synthesized by impregnation of a calcium nitrate solution on a nanostructured calcium silicate matrix (see Fig. 10), which acted as a thermally stable support for CaO. Similarly, it may be argued that the thermal stability and enhanced porosity provided by the nanostructured MgO skeleton in the case of cal-

280 cined dolomite allows the capture capacity of the dolomite derived sorbent to outweigh the  
281 performance of limestone derived CaO, which is critically impaired when regenerated by  
282 calcination under severe realistic conditions.

283 In some of the SEM images obtained in our work there is a marked segregation between  
284 the MgO nanostructured grains and the sintered CaO skeleton. This is particularly notice-  
285 able in the case of dolomite samples subjected to carb/recarb/carb cycles (precalcined and  
286 regenerated under severe conditions) as may be seen in Fig. 11. Since diffusivity is enhanced  
287 under the conditions of recarbonation (high temperature and high CO<sub>2</sub> concentration) [47–  
288 49], it is likely that the segregation of MgO and CaO grains is promoted in accordance with  
289 the mechanism reported elsewhere from in-situ observations [21]. This would lead to a loss  
290 of efficiency of the MgO skeleton on enhancing the sorbent capture capacity, which can be  
291 the reason for the observed slight decline of capture capacity performance of the dolomite  
292 sample precalcined under severe conditions and subjected to a recarbonation stage (Fig.  
293 6b). SEM pictures of cycled limestone and dolomite samples under diverse conditions can  
294 be seen in Fig. 12 and show in general a higher porosity of the CaO skeleton for dolomite in  
295 accordance with the higher conversion exhibited by this sorbent. Remarkably, MgO grains  
296 are not visible in the surface of the cycled dolomite samples shown in Fig. 12. Figure 13  
297 illustrate more clearly this phenomenon usually observed in the SEM pictures. Presumably,  
298 repeated carbonation/calcinations on the surface of the particles and significant sintering  
299 of the nascent CaO grains supported on the inert MgO skeleton would be responsible for  
300 this segregation. As may be seen in these pictures, MgO grains have a tendency to migrate  
301 towards the interior of the particles whereas sintered CaO grains build up onto the surface of  
302 the particles. This kind of segregation is clearly observed in the representative photographs  
303 on the right of Fig. 13, where the cross section of a fractured particle is featured.

#### 304 IV. KINETICS OF LIMESTONE AND DOLOMITE CALCINATION

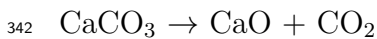
305 Simulations of the CaL technology at the industrial level show that the energy demand  
306 in the calciner can reach a fraction near half the total energy required in the process [11] or  
307 even higher if the detrimental effect on limestone performance caused by regeneration under  
308 high CO<sub>2</sub>% were taken into account. Many research efforts are thus currently devoted to  
309 the development of innovative techniques to achieve a high calciner efficiency at a decreased  
310 temperature and taking into account the short residence times imposed [15, 28]. Our goal in  
311 this section is to carry out a comparative analysis of the decarbonation kinetics of limestone  
312 and dolomite during calcination in our TGA tests.

313 As seen in Fig. 14 limestone and dolomite follow very similar decarbonation kinetics  
314 when calcined in air by slowly increasing the temperature up to 850°C. In agreement with  
315 observations reported in the literature [50, 51], we see that decarbonation of dolomite in air  
316 occurs in one stage and starts at about 600°C analogously to limestone. Figure 15 illustrates  
317 the kinetics of limestone calcination under 70%CO<sub>2</sub> by quickly increasing the temperature up  
318 to 950°C. As may be seen, the presence of CO<sub>2</sub> hinders severely decarbonation of limestone  
319 as widely reported in the literature [39, 52–58]. Since CaCO<sub>3</sub> decarbonation is heavily  
320 influenced by the thermodynamic equilibrium the presence of CO<sub>2</sub> displaces it to higher  
321 temperatures but also slows down it markedly. Decarbonation is seen to start in Fig. 15  
322 at about 900°C (around 30°C above the thermodynamic equilibrium temperature under  
323 70%CO<sub>2</sub> at atmospheric pressure [39]) and only progresses at a sufficiently fast rate to  
324 be fully attained in a short residence time if the calcination temperature is raised above  
325 925°C in accordance with pilot-scale tests results [3, 7–10]. As compared to limestone,  
326 the kinetics of dolomite calcination under 70%CO<sub>2</sub> shows radically different features as

327 may be observed in Fig. 16. In agreement with previous works [50, 51], decomposition of  
328 dolomite under high CO<sub>2</sub> concentration is seen to occur mainly by two stages. Irreversible  
329 MgCO<sub>3</sub> decomposition occurs in a first stage whereas the second stage involving CaCO<sub>3</sub>  
330 decomposition is initiated at around 650°C, which is well below the equilibrium temperature  
331 for pure CaCO<sub>3</sub> decomposition. As shown in Fig. 16, decarbonation of dolomite is fully  
332 achieved in a time period below 5 minutes at a calcination temperature of just 900°C.

333 The thermal decomposition of dolomite via a single step at low partial pressures of CO<sub>2</sub>  
334 and along two distinct stages at high CO<sub>2</sub> partial pressures observed in our work is a well  
335 documented phenomenon, yet the mechanism responsible for this behavior is still a subject  
336 of debate [19–21, 23, 51, 59–61]. Experimental studies have shown that the intermediate  
337 products between stages in the decomposition process under CO<sub>2</sub> are MgCO<sub>3</sub>, CaCO<sub>3</sub> and  
338 MgO while the final products were CaO and MgO. Thus, it is usual to represent the process  
339 by means of the reactions

340



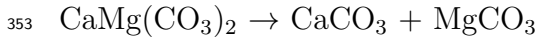
343

344 De-mixing of Ca<sup>2+</sup> and Mg<sup>2+</sup> cations in the 1st stage (half-decomposition) is thought  
345 to yield the nucleation and growth of MgO crystals resistant to sintering and the con-  
346 comitant formation of CaCO<sub>3</sub> through the diffusion of its constituents within the lattice.  
347 Solid-state diffusion (of cations in the lattice and of CO<sub>3</sub><sup>2-</sup> across the reacting interface) are  
348 thus believed to be the rate-limiting factors of half-decomposition. As a matter of fact, it  
349 is reported that the half-decomposition temperature is considerably decreased by grinding  
350 the dolomite sample [51], which is known to decrease the resistance to solid-state diffusion



351 [48, 49]. An alternative more compact representation of the reaction is [59]

352



354

355 being  $\text{MgCO}_3$  thermodynamically unstable at relatively lower temperatures [23], which  
356 gives rise to the two-stage decomposition process. In accordance with this formulation we  
357 see that the 1st weight loss (Fig. 16) occurs within the temperature range 400–500°C, which  
358 conforms to the equilibrium temperature of  $\text{MgCO}_3$  decomposition at a  $\text{CO}_2$  partial pressure  
359 of 0.7 atm [23] (70% vol concentration at atmospheric pressure in our tests). Nonetheless,  
360 half-decomposition is generally observed at higher temperatures [60] in experiments usually  
361 carried out at low heating rates ( $\sim 10^\circ\text{C}/\text{min}$ ). In our tests, 1st chemical decomposition  
362 is triggered just when the heating rate is increased to  $300^\circ\text{C}/\text{min}$ , which suggests that the  
363 heating rate plays a relevant role on the mechanism of the process. On the other hand, Fig.  
364 16 shows that  $\text{MgO}\cdot\text{CaCO}_3$  decomposition would be started at temperatures well below the  
365 equilibrium temperature for pure  $\text{CaCO}_3$  decomposition ( $T_{eq} \approx 870^\circ\text{C}$ ) whereas the kinetics  
366 of  $\text{MgO}\cdot\text{CaCO}_3$  decomposition would be significantly enhanced as compared to limestone  
367 decomposition under  $\text{CO}_2$ .

368 Figure 17 illustrates the kinetics of  $\text{CaCO}_3$  and  $\text{MgO}\cdot\text{CaCO}_3$  decomposition during  $\text{CaO}$   
369 regeneration in the 1st carb/calc cycle. As opposed to the contrasting behaviors exhibited  
370 by limestone and dolomite calcination, it is observed that the calcination kinetics for both  
371 sorbents is similar in this regeneration stage under high  $\text{CO}_2$  concentration. Decarbonation  
372 commences at about  $850^\circ\text{C}$  and proceeds at a quick rate, which is still faster for the dolomite  
373 derived sorbent. Arguably, desorption of  $\text{CO}_2$  at high  $\text{CO}_2$  partial pressure would be favored  
374 across the boundaries between different phases. The  $\text{CaCO}_3/\text{CaO}$  transformation experi-

375 enced by both sorbents during regeneration would be thus governed by a similar mechanism  
376 with the MgO grains serving as a stable nano-structured support for the dolomite derived  
377 CaO and favoring solid-state diffusion.

## 378 V. CAO REGENERATION AND SINTERING

379 The loss of multicyclic CaO conversion is usually explained from the marked sintering  
380 suffered by the CaO skeleton regenerated by calcination at high temperature [41, 43]. The  
381 point at which sintering begins in ceramic materials occurs at the Tammann temperature,  
382 which, as a rule of thumb, is considered as half their melting temperature. As seen in our  
383 SEM pictures, CaO grains of dolomite samples subjected to repeated carb/cal cycles exhibit  
384 indeed notable sintering, yet MgO grains appear resistant to sintering. This is a puzzling  
385 observation if one takes into account that the Tammann temperatures of both oxides are not  
386 very different ( $T_t \simeq 1170^\circ\text{C}$  for CaO and  $T_t \simeq 1276^\circ\text{C}$  for MgO) [16] and both are well over  
387 the calcination temperature at CaL conditions. However, the main reason for the sintering  
388 dissimilarity of both oxides must be sought in their different multicyclic history. The essential  
389 issue is that CaO undergoes repeated carbonation and regenerations whereas MgO remains  
390 as an inert oxide. It may be therefore hypothesized that most of CaO sintering occurs  
391 during the  $\text{CaCO}_3/\text{CaO}$  transformation in each cycle. Figure 18 shows limestone derived  
392 CaO conversion data from carb/calc cycles in which the calcination stages were prolonged  
393 to 3 hours. As may be seen, and despite the excessively long calcination periods, CaO  
394 conversion is not remarkably decreased as compared to conversion in the tests with short  
395 calcination stages (5 min) mimicking practical conditions, which supports the argument  
396 that sintering and deactivation occurs mostly in the nascent CaO during the  $\text{CaCO}_3/\text{CaO}$   
397 transformation and not after CaO has reached its stable form.

398 Empirical measurements reported in a wide number of works indicate that the sintering  
399 of CaO is greatly accelerated when CO<sub>2</sub> is present in the calcination atmosphere at high  
400 concentration [42, 57, 62] whereas the CaCO<sub>3</sub> decarbonation rate suffers a drastic decline  
401 [39, 52–58]. Gaining understanding on the physicochemical mechanism behind this behav-  
402 ior should be a main scientific focus of studies on the CaL process since it determines the  
403 multicyclic sorbent performance and therefore has a great influence on the efficiency of the  
404 technology. Decarbonation of CaCO<sub>3</sub> is initiated by the chemical decomposition of CaCO<sub>3</sub>  
405 to yield CaO and CO<sub>2</sub> adsorbed, which is afterwards desorbed [39, 52]. At low CO<sub>2</sub> partial  
406 pressures, the process is rate limited by the chemical decomposition stage since desorption is  
407 very fast [39]. In the case of high CO<sub>2</sub> partial pressure however, CO<sub>2</sub> desorption is severely  
408 hampered and would limit the decarbonation process [56]. Empirical studies indicate that  
409 the presence of CO<sub>2</sub> at high concentrations in the calcination atmosphere leads to a reversible  
410 CO<sub>2</sub> desorption/adsorption dynamic process [53, 56] that would slow down decarbonation.  
411 In the pioneer work of Hyatt et al. [52], experimental measurements on the rate of cal-  
412 cite crystals calcination lead the authors to formulate the hypothesis that the nascent CaO  
413 lattice acquires a metastable rhombohedral structure (similar to the original CaCO<sub>3</sub>) when  
414 CO<sub>2</sub> is desorbed, after which the stable CaO cubic lattice nucleates from the transforma-  
415 tion of the metastable CaO, which acts as bridge for the reaction. Later results from XRD  
416 analysis upheld the idea that a distorted metastable phase of CaO was formed during de-  
417 carbonation of calcite [63, 64] although little could be concluded about its crystal structure.  
418 A more recent study [65] has shown from diverse advanced characterization techniques that  
419 the CaCO<sub>3</sub>/CaO transformation starts by the formation of a mesoporous structure made up  
420 of rod-shaped (metastable) CaO nanocrystals on each rhombohedral cleavage face of the cal-  
421 cite pseudomorph. These CaO nanocrystals undergo oriented aggregation driven by van der

422 Waals attractive forces to minimize surface energy. Aggregated nanocrystals become after-  
423 wards sintered as decomposition progresses. Oriented aggregation and sintering reduces the  
424 surface area and porosity of the metastable structure by closing the mesopores between the  
425 rod-shaped CaO nanocrystals, which results in the formation of macropores through which  
426 CO<sub>2</sub> can easily escape to complete the transformation by the nucleation of stable CaO cubic  
427 crystals [65]. Chemical decomposition was observed to control the kinetics of the process  
428 during most of the CaCO<sub>3</sub>/CaO transformation in these experiments [65], which were car-  
429 ried out in vacuum and air. Under these conditions there is no significant resistance against  
430 CO<sub>2</sub> diffusion to migrate outside the metastable CaO structure. However, the resistance for  
431 CO<sub>2</sub> to escape the metastable CaO mesoporous structure by diffusion would be impaired  
432 under a high CO<sub>2</sub> partial pressure in the environment outside the solid, which would favor  
433 re-adsorption of CO<sub>2</sub>. It is well known that adsorption of CO<sub>2</sub> on solid surfaces gives rise to a  
434 significant increase of the surface energy and therefore enhances the attractive force between  
435 the solids [66]. Thus, it may be expected that, in the presence of CO<sub>2</sub> adsorbed onto the  
436 surfaces of metastable CaO nanocrystals, their aggregation is promoted, which would favor  
437 their subsequent sintering. In regards to decarbonation during regeneration of MgO·CaCO<sub>3</sub>,  
438 it may be argued that the presence of inert MgO nanocrystals between the CaO metastable  
439 nanocrystals would reduce their attractive forces, thus counteracting the effect of high CO<sub>2</sub>  
440 partial pressure by preventing their adhesive aggregation and subsequent sintering. As the  
441 number of cycles progresses, the cumulative aggregation and sintering of CaO nanocrys-  
442 tals in each CaCO<sub>3</sub>/CaO transformation would lead to a segregation between the sintered  
443 CaO skeleton and the resistant to sintering MgO grains as observed from our SEM analysis.  
444 Moreover, this argument may explain why sintered CaO is mostly seen on the surface of  
445 cycled dolomite particles since it is there where most of CaO carbonation/regeneration takes

446 place in short residence times. Further research must be devoted in future works to explore  
447 the fundamental mechanism of  $\text{CaCO}_3/\text{CaO}$  transformation at high  $\text{CO}_2$  pressure but it  
448 seems clear that the multicyclic loss of  $\text{CaO}$  conversion when subjected to repeated carb/cal  
449 cycles is determined by the evolution of metastable  $\text{CaO}$  formed during the  $\text{CaCO}_3/\text{CaO}$   
450 transformation in each regeneration stage. From the practical point of view, it would be  
451 interesting to devise feasible strategies to tailor this transformation by minimizing aggrega-  
452 tion and sintering of metastable  $\text{CaO}$  nanocrystals. Presumably, this is the role played by  
453 the  $\text{MgO}$  inert grains in natural dolomite.

## 454 **VI. INFLUENCE OF SORBENT PERFORMANCE ON THE CAL TECHNOLOGY EFFICIENCY**

455

456 Leaving aside the question on the fundamental mechanism that governs limestone and  
457 dolomite decompositions under high  $\text{CO}_2$  concentration, our results suggest that the use  
458 of dolomite in the CaL technology would allow decreasing the temperature of the calciner  
459 significantly. In regards to limestone, process simulations [8] show that the minimum cal-  
460 cination temperature to achieve an acceptable calciner efficiency would be above  $930^\circ\text{C}$   
461 whereas the calciner efficiency would be severely hampered if the temperature is decreased  
462 to  $900^\circ\text{C}$ , which agrees with our observations on the kinetics of limestone decarbonation  
463 under high  $\text{CO}_2$  concentration. On the other hand, our results indicate that a sufficiently  
464 high calciner efficiency would be attainable at  $900^\circ\text{C}$  if natural dolomite is used, which de-  
465 composes quickly at this reduced temperature under a high  $\text{CO}_2$  concentration environment.  
466 According to process simulation results [11] a decrease of the calcination temperature from  
467  $950^\circ\text{C}$  to  $900^\circ\text{C}$  (while maintaining a high calciner efficiency) may bring about a substantial  
468 reduction of costs. Particularly, the amounts of coal and oxygen needed for oxy-combustion

469 to raise the calciner temperature and the additional CO<sub>2</sub> produced by oxy-combustion,  
470 which represent an important penalty for the technology [13, 28], would be lowered. Process  
471 simulations [13, 45] indicate that the ratio of the mass of coal needed for oxy-combustion  
472 to the mass of CO<sub>2</sub> captured would be decreased by a 10% if the calciner temperature is  
473 decreased from 950°C to 900°C in the ordinary CaL configuration. If limestone is used,  
474 the calciner temperature should be kept at 950°C and a similar 10% reduction would be  
475 possible by incorporating a cyclonic preheater to transfer heat from hot gas leaving the cal-  
476 ciner to the solids coming out from the carbonator, which has been proposed as a feasible  
477 innovation to improve the industrial competitiveness of the technology [13]. Process simu-  
478 lations indicate also that a low calciner to carbonator inventory ratio (of about 0.2) would  
479 be only possible for limestone by calcining at 950°C (which yields a high calciner efficiency)  
480 whereas a decrease of the calciner temperature to 900°C would require increasing this ratio  
481 to about 1.2 [13]. Since full decarbonation at realistic CaL conditions could be efficiently  
482 attained at 900°C for dolomite, it may be expected that the use of dolomite would allow  
483 for a considerable reduction of the solids inventory in the calciner further decreasing the  
484 energy penalty of the technology. Process simulations also show that the CaO/CO<sub>2</sub> molar  
485 ratio ( $R$ ) can be substantially decreased by a decrease of the calcination temperature for a  
486 constant purge flow of solids ( $f$ ) and if the capture efficiency ( $\eta$ ) is kept constant as would  
487 be possible by using dolomite. For example, for  $f = 3\%$  and  $\eta = 0.85$ , it would be  $R \simeq 10$   
488 at 950°C and  $R \simeq 7.5$  at 900°C [13]. The amount of solids purge and make-up flows have a  
489 relevant influence on the process performance [12, 31]. Large purge flows lead to a dramatic  
490 increase of the heat demand for calcination and hence the cost for oxygen production and  
491 auxiliaries consumption is raised. Thus, the cost of CO<sub>2</sub> avoided tonne (tCO<sub>2</sub>) is minimized  
492 at relatively low purges. At an optimum CaO/CO<sub>2</sub> molar ratio of  $R = 5$  and only  $f = 1\%$

493 purge the estimated cost is around 14/tCO<sub>2</sub> whereas an increase of the purge flow in the  
494 calciner (as would be required by enhanced deactivation) to 2.5% would increase the tCO<sub>2</sub>  
495 avoided cost by  $\sim 1$  /tCO<sub>2</sub> [31].

496 An additional important aspect to be carefully addressed in future TGA studies on lime-  
497 stone and dolomite at realistic CaL conditions is the irreversible sulphation of the sorbent  
498 due to the presence of SO<sub>2</sub> either in the flue gas in the carbonator or in the calciner due  
499 to oxy-combustion, which causes a notable decay of CaO conversion [10, 27, 67]. The main  
500 factor limiting CaO sulphation reactivity is pore blocking [68–70]. Sulphation is essentially  
501 favored by sintering and hence sulphation conversion is observed to increase with the cycle  
502 number in multicyclic carb/cal tests [9]. Since CaO sintering is mitigated in the dolomite  
503 derived sorbent, sulphation would be presumably minimized by the use of dolomite as com-  
504 pared to limestone. Moreover, the possibility of lowering down the calciner temperature  
505 would allow decreasing the generation of SO<sub>2</sub> in this reactor, which would serve to further  
506 mitigate deactivation of the sorbent as caused by sulphation thus allowing for a reduction  
507 of the makeup of fresh solids to counterbalance the purge flow of the solids deactivated.  
508 Moreover, as seen in our work (Fig. 2b), the capture capacity of dolomite is substantially  
509 higher than that of limestone for the initial solids inventory precalcined in air, which would  
510 allow further decreasing the amount of purged solids while the capture efficiency is kept at  
511 a high level [31]. On the other hand, our results show (section III A) that, for the solids  
512 precalcined under high CO<sub>2</sub> concentration, the multicyclic capture behavior of dolomite in  
513 ordinary carb/calc cycles is similar to that of limestone when an intermediate recarbonation  
514 stage is introduced with the goal of reducing the amount of purged solids to a minimum  
515 required for desulfurization as proposed elsewhere [33–35]. Simulations of a large-scale sys-  
516 tem indicate that a bubbling recarbonator reactor with a cross-sectional area of between 80

517 and 100 m<sup>2</sup>, expanded bed height of 2 m, and inlet gas velocities of 0.6 - 0.9 m/s would  
518 be needed for this purpose [71]. According to simulations, by introducing a recarbonator  
519 reactor, the make-up flow of limestone would be as low as 0.07 kg limestone per kg coal as  
520 compared to 0.35 kg limestone per kg coal predicted in the ordinary CaL configuration [33],  
521 which would lead to a significant reduction in energy consumption and coal/oxygen for oxy-  
522 combustion (albeit it must be reminded that these simulations were based on the assumption  
523 of a sorbent behavior inferred from TGA tests in which the samples were regenerated un-  
524 der low CO<sub>2</sub> concentration [33, 35]). Since, as observed in our work, the performance of  
525 dolomite subjected to ordinary carb/calc cycle is similar to that of limestone subjected to  
526 carb/recarb/calc cycles, the reduction of costs by using dolomite instead of limestone could  
527 be estimated from the costs involving the incorporation of an additional recarbonator reac-  
528 tor to reactivate the limestone derived CaO, which should be re-assessed by considering the  
529 sorbents behavior under realistic regeneration conditions. A potential issue related to the  
530 use of dolomite in the CaL technology is its friability as suggested in some works [27], which  
531 may be due to the development of intense residual stresses inside the porous matrix of the  
532 solid during decomposition [19] also leading to decrepitation phenomena observed in TGA  
533 tests [59, 72]. Particle fragmentation would occur however only during dolomite decompo-  
534 sition and not in the sorbent regeneration stage. Accordingly, the rate of generation of fine  
535 particle fragments in lab-scale fluidized bed tests [27] has been observed to be significant  
536 just in the first calcination.

## 537 VII. CONCLUSIONS

538 A main conclusion of our study is that natural dolomite can be an advantageous alterna-  
539 tive to limestone as sorbent precursor for postcombustion CO<sub>2</sub> capture by means of the CaL



540 technology. TGA tests carried out under realistic sorbent regeneration conditions (high CO<sub>2</sub>  
541 concentration, high temperature and quick transitions between carbonation and calcination  
542 stages) show that the capture capacity of limestone derived CaO is critically influenced by  
543 precalcination conditions and an intermediate recarbonation stage. The capture capacity  
544 of CaO derived from precalcining limestone in air suffers a drastic drop in the first cycles.  
545 Moreover, the introduction of a recarbonation stage, which is intended in practice to mini-  
546 mize the need for a makeup flow of fresh limestone fed to the calciner, would actually have  
547 an adverse effect on the capture capacity of the sorbent derived from precalcining the initial  
548 inventory of limestone in air. SEM analysis of CaO derived from limestone precalcined in  
549 air and regenerated under high CO<sub>2</sub> concentration/high temperature show that it suffers  
550 marked sintering. The multicyclic stability of CaO may be enhanced if precalcination is  
551 carried out under the same conditions as those used for regeneration, which leads also to a  
552 favorable effect of recarbonation. On the other hand, the behavior of the sorbent derived  
553 from dolomite is quite insensitive to either precalcination or recarbonation conditions and  
554 shows a neatly higher capture capacity as compared to limestone at realistic calcination  
555 conditions. The predictability of dolomite behavior, regardless of precalcination and recar-  
556 bonation conditions, can be a further advantage over the strong dependence of limestone  
557 performance on these conditions, which may vary uncontrollably in any modification of the  
558 process. For example, proposed innovations of the CaL technology such as the addition of  
559 a cyclonic preheater to transfer heat from the hot gas leaving the calciner to the particles  
560 exiting the carbonator [13] will lead to recarbonation of the partially carbonated solids. In  
561 this case, and if the makeup flow of fresh limestone fed to the calciner is minimized, the  
562 activity of the sorbent precalcined in air might be further hindered. SEM analysis demon-  
563 strates that, after a number of carbonation/calcination cycles, MgO and CaO grains in

564 the dolomite samples become segregated with resistant to sintering MgO grains migrating  
565 towards the interior of the particles and a CaO layer building up on their surface. The  
566 improved stability provided by the inert MgO skeleton would serve to significantly enhance  
567 the multicyclic CaO conversion and sorbent capture capacity at realistic CaL conditions for  
568 postcombustion CO<sub>2</sub> capture. An additional potential advantage brought about by the use  
569 of dolomite would be its much faster decomposition under CO<sub>2</sub> as compared to limestone,  
570 which would allow reducing notably the temperature of the calciner that imposes the main  
571 energy penalty to the technology.

## 572 **VIII. ACKNOWLEDGEMENTS**

573 This work was supported by the Andalusian Regional Government Junta de Andalucia  
574 (contracts FQM-5735, TEP-7858 and TEP-1900), Spanish Government Agency Ministerio  
575 de Economia y Competitividad and FEDER funds (contracts FIS2011-25161 and CTQ2011-  
576 27626). One of the authors (PESJ) is supported by the Juan de la Cierva program of the  
577 Spanish Ministerio de Economia y Competitividad. We gratefully acknowledge the XRD and  
578 SEM services of the Innovation, Technology and Research Center of the University of Seville  
579 (CITIUS). The valuable assistance of Dr. Francisco Varela (CITIUS) with the microscopy  
580 analysis and fruitful discussions with Drs. Luis M Romeo and Pilar Lisbona (University of  
581 Zaragoza-CIRCE) are warmly appreciated.

- 
- 583 [1] J. Blamey, E. J. Anthony, J. Wang, and P. S. Fennell, “The calcium looping cycle for large-  
584 scale CO<sub>2</sub> capture,” *Prog. Energ. Combust. Sci.*, vol. 36, no. 2, pp. 260–279, 2010.
- 585 [2] M. C. Romano, “Modeling the carbonator of a Ca-looping process for CO<sub>2</sub> capture from power  
586 plant flue gas,” *Chemical Engineering Science*, vol. 69, pp. 257 – 269, 2012.
- 587 [3] B. Arias, M. Diego, J. Abanades, M. Lorenzo, L. Diaz, D. Martinez, J. Alvarez, and  
588 A. Sanchez-Biezma, “Demonstration of steady state CO<sub>2</sub> capture in a 1.7 MWth calcium  
589 looping pilot,” *International Journal of Greenhouse Gas Control*, vol. 18, pp. 237–245, 2013.
- 590 [4] M. C. Romano, I. Martinez, R. Murillo, B. Arstad, R. Blom, D. C. Ozcan, H. Ahn, and  
591 S. Brandani, “Process simulation of Ca-looping processes: review and guidelines,” *Energy  
592 Procedia*, vol. 37, pp. 142 – 150, 2013.
- 593 [5] M.-H. Chang, C.-M. Huang, W.-H. Liu, W.-C. Chen, J.-Y. Cheng, W. Chen, T.-W. Wen,  
594 S. Ouyang, C.-H. Shen, and H.-W. Hsu, “Design and experimental investigation of Calcium  
595 Looping process for 3-kWth and 1.9-MWth facilities,” *Chemical Engineering & Technology*,  
596 vol. 36, no. 9, pp. 1525–1532, 2013.
- 597 [6] J. Ströhle, M. Junk, J. Kremer, A. Galloy, and B. Epple, “Carbonate looping experiments in  
598 a 1MWth pilot plant and model validation,” *Fuel*, vol. 127, no. 0, pp. 13 – 22, 2014. Fluidized  
599 Bed Combustion and Gasification CO<sub>2</sub> and SO<sub>2</sub> capture: Special Issue in Honor of Professor  
600 E.J. (Ben) Anthony.
- 601 [7] A. Charitos, N. Rodriguez, C. Hawthorne, M. Alonso, M. Zieba, B. Arias, G. Kopanakis,  
602 G. Scheffknecht, and J. C. Abanades, “Experimental validation of the Calcium Looping CO<sub>2</sub>

- 603 capture process with two circulating fluidized bed carbonator reactors,” *Industrial & Engi-*  
604 *neering Chemistry Research*, vol. 50, no. 16, pp. 9685–9695, 2011.
- 605 [8] I. Martinez, G. Grasa, R. Murillo, B. Arias, and J. Abanades, “Modelling the continuous  
606 calcination of  $\text{CaCO}_3$  in a Ca-looping system,” *Chemical Engineering Journal*, vol. 215–216,  
607 pp. 174–181, 2013.
- 608 [9] R. T. Symonds, D. Y. Lu, V. Manovic, and E. J. Anthony, “Pilot-scale study of  $\text{CO}_2$  capture  
609 by cao-based sorbents in the presence of steam and  $\text{SO}_2$ ,” *Industrial & Engineering Chemistry*  
610 *Research*, vol. 51, no. 21, pp. 7177 – 7184, 2012.
- 611 [10] A. Coppola, F. Scala, P. Salatino, and F. Montagnaro, “Fluidized bed calcium looping cycles  
612 for  $\text{CO}_2$  capture under oxy-firing calcination conditions: Part 1. assessment of six limestones,”  
613 *Chemical Engineering Journal*, vol. 231, pp. 537 – 543, 2013.
- 614 [11] N. Rodriguez, M. Alonso, G. Grasa, and J. C. Abanades, “Heat requirements in a calciner  
615 of  $\text{CaCO}_3$  integrated in a  $\text{CO}_2$  capture system using  $\text{CaO}$ ,” *Chemical Engineering Journal*,  
616 vol. 138, no. 1–3, pp. 148–154, 2008.
- 617 [12] L. M. Romeo, Y. Lara, P. Lisbona, and J. M. Escosa, “Optimizing make-up flow in a  $\text{CO}_2$   
618 capture system using  $\text{CaO}$ ,” *Chemical Engineering Journal*, vol. 147, no. 2-3, pp. 252 – 258,  
619 2009.
- 620 [13] A. Martinez, Y. Lara, P. Lisbona, and L. M. Romeo, “Operation of a cyclonic preheater  
621 in the Ca-looping for  $\text{CO}_2$  capture,” *Environmental Science & Technology*, vol. 47, no. 19,  
622 pp. 11335–11341, 2013.
- 623 [14] J. M. Valverde, P. E. Sanchez-Jimenez, and L. A. Perez-Maqueda, “Calcium-looping for post-  
624 combustion  $\text{CO}_2$  capture. on the adverse effect of sorbent regeneration under  $\text{CO}_2$ ,” *Applied*  
625 *Energy*, vol. 126, pp. 161–171, 2014.

- 626 [15] J. Ylatalo, J. Ritvanen, T. Tynjala, and T. Hyppanen, “Model based scale-up study of the  
627 calcium looping process,” *Fuel*, vol. 115, pp. 329–337, 2014.
- 628 [16] A. M. Kierzkowska, R. Pacciani, and C. R. Müller, “CaO-based CO<sub>2</sub> sorbents: From funda-  
629 mentals to the development of new, highly effective materials,” *ChemSusChem*, vol. 6, no. 7,  
630 pp. 1130–1148, 2013.
- 631 [17] J. M. Valverde, “Ca-based synthetic materials with enhanced CO<sub>2</sub> capture efficiency,” *J.*  
632 *Mater. Chem. A.*, vol. 1, p. 447–468, 2013.
- 633 [18] J. E. Readman and R. Blom, “The use of in situ powder X-ray diffraction in the investigation  
634 of dolomite as a potential reversible high-temperature CO<sub>2</sub> sorbent,” *Phys. Chem. Chem.*  
635 *Phys.*, vol. 7, pp. 1214–1219, 2005.
- 636 [19] D. Beruto, R. Vecchiattini, and M. Giordani, “Effect of mixtures of H<sub>2</sub>O (g) and CO<sub>2</sub> (g)  
637 on the thermal half decomposition of dolomite natural stone in high CO<sub>2</sub> pressure regime,”  
638 *Thermochimica Acta*, vol. 404, no. 1–2, pp. 25–33, 2003.
- 639 [20] H. Galai, M. Pijolat, K. Nahdi, and M. Trabelsi-Ayadi, “Mechanism of growth of MgO and  
640 CaCO<sub>3</sub> during a dolomite partial decomposition,” *Solid State Ionics*, vol. 178, no. 15–18,  
641 pp. 1039 – 1047, 2007.
- 642 [21] C. Rodriguez-Navarro, K. Kudlacz, and E. Ruiz-Agudo, “The mechanism of thermal decompo-  
643 sition of dolomite: New insights from 2D-XRD and TEM analyses,” *American Mineralogist*,  
644 vol. 97, pp. 38–51, 2012.
- 645 [22] K. Chrissafis, C. Dagounaki, and K. Paraskevopoulos, “The effects of procedural variables on  
646 the maximum capture efficiency of CO<sub>2</sub> using a carbonation/calcination cycle of carbonate  
647 rocks,” *Thermochimica Acta*, vol. 428, no. 12, pp. 193 – 198, 2005.

- 648 [23] A. Silaban, M. Narcida, and D. P. Harrison, “Characteristics of the reversible reaction be-  
649 tween  $\text{CO}_2(\text{g})$  and calcined dolomite,” *Chemical Engineering Communications*, vol. 146, no. 1,  
650 pp. 149–162, 1996.
- 651 [24] K. O. Albrecht, K. S. Wagenbach, J. A. Satrio, B. H. Shanks, and T. D. Wheelock, “Devel-  
652 opment of a  $\text{CaO}$ -based  $\text{CO}_2$  sorbent with improved cyclic stability,” *Ind. Eng. Chem. Res.*,  
653 vol. 47, p. 7841–7848, 2008.
- 654 [25] D. S. Sultan, C. R. Muller, and J. S. Dennis, “Capture of  $\text{CO}_2$  using sorbents of calcium  
655 magnesium acetate (CMA),” *Energy & Fuels*, vol. 24, no. 6, pp. 3687–3697, 2010.
- 656 [26] X. Yang, L. Zhao, S. Yang, and Y. Xiao, “Investigation of natural  $\text{CaO-MgO}$  sorbent for  $\text{CO}_2$   
657 capture,” *Asia-Pacific Journal of Chemical Engineering*, vol. 8, no. 6, pp. 906–915, 2013.
- 658 [27] A. Coppola, F. Scala, P. Salatino, and F. Montagnaro, “Fluidized bed calcium looping cycles  
659 for  $\text{CO}_2$  capture under oxy-firing calcination conditions: Part 2. assessment of dolomite vs.  
660 limestone,” *Chemical Engineering Journal*, vol. 231, pp. 544–549, 2013.
- 661 [28] J. Ylatalo, J. Parkkinen, J. Ritvanen, T. Tynjala, and T. Hyppanen, “Modeling of the oxy-  
662 combustion calciner in the post-combustion calcium looping process,” *Fuel*, vol. 113, pp. 770–  
663 779, 2013.
- 664 [29] N. Rodriguez, M. Alonso, J. C. Abanades, A. Charitos, C. Hawthorne, G. Scheffknecht, D. Y.  
665 Lu, and E. J. Anthony, “Comparison of experimental results from three dual fluidized bed  
666 test facilities capturing  $\text{CO}_2$  with  $\text{CaO}$ ,” *Energy Procedia*, vol. 4, pp. 393–401, 2011.
- 667 [30] F. Pontiga, J. M. Valverde, H. Moreno, and F. J. Duran-Olivencia, “Dry gassolid carbonation  
668 in fluidized beds of  $\text{Ca}(\text{OH})_2$  and nanosilica/ $\text{Ca}(\text{OH})_2$  at ambient temperature and low  $\text{CO}_2$   
669 pressure,” *Chemical Engineering Journal*, vol. 222, pp. 546–552, 2013.

- 670 [31] L. M. Romeo, Y. Lara, P. Lisbona, and A. Martinez, “Economical assessment of competitive  
671 enhanced limestones for CO<sub>2</sub> capture cycles in power plants,” *Fuel Processing Technology*,  
672 vol. 90, no. 6, pp. 803 – 811, 2009.
- 673 [32] I. Martnez, G. Grasa, R. Murillo, B. Arias, and J. Abanades, “Modelling the continuous  
674 calcination of CaCO<sub>3</sub> in a Ca-looping system,” *Chemical Engineering Journal*, vol. 215-216,  
675 pp. 174–181, 2013.
- 676 [33] B. Arias, G. S. Grasa, M. Alonso, and J. C. Abanades, “Post - combustion calcium looping  
677 process with a highly stable sorbent activity by recarbonation,” *Energy Environ. Sci.*, vol. 5,  
678 pp. 7353 – 7359, 2012.
- 679 [34] M. E. Diego, B. Arias, M. Alonso, and J. C. Abanades, “The impact of calcium sulfate and  
680 inert solids accumulation in post-combustion calcium looping systems,” *Fuel*, vol. 109, pp. 184  
681 – 190, 2013.
- 682 [35] G. Grasa, I. Martnez, M. E. Diego, and J. C. Abanades, “Determination of CaO carbonation  
683 kinetics under recarbonation conditions,” *Energy & Fuels*, vol. 28, no. 6, p. 4033–4042, 2014.
- 684 [36] J. M. Valverde, P. E. Sanchez Jimenez, and L. A. Perez Maqueda, “High and stable CO<sub>2</sub>  
685 capture capacity of natural limestone at Ca-looping conditions by heat pretreatment and  
686 recarbonation synergy,” *Fuel*, vol. 123, pp. 79–85, 2014.
- 687 [37] J. M. Valverde, P. E. Sanchez-Jimenez, and L. A. Perez-Maqueda, “Effect of heat pretreat-  
688 ment/recarbonation in the Ca-looping process at realistic calcination conditions,” *Energy &*  
689 *Fuels*, vol. 28, no. 6, pp. 4062–4067, 2014.
- 690 [38] M. Alonso, Y. Criado, J. Abanades, and G. Grasa, “Undesired effects in the determination of  
691 CO<sub>2</sub> carrying capacities of CaO during TG testing,” *Fuel*, vol. 127, pp. 52–61, 2014.

- 692 [39] F. Garcia-Labiano, A. Abad, L. de Diego, P. Gayan, and J. Adanez, “Calcination of calcium-  
693 based sorbents at pressure in a broad range of CO<sub>2</sub> concentrations,” *Chemical Engineering*  
694 *Science*, vol. 57, no. 13, pp. 2381 – 2393, 2002.
- 695 [40] G. Grasa, R. Murillo, M. Alonso, and J. C. Abanades, “Application of the random pore model  
696 to the carbonation cyclic reaction,” *AIChE J.*, vol. 55, no. 5, pp. 1246–1255, 2009.
- 697 [41] G. S. Grasa and J. C. Abanades, “CO<sub>2</sub> capture capacity of CaO in long series of carbona-  
698 tion/calcination cycles,” *Ind. Eng. Chem. Res.*, vol. 45, no. 26, pp. 8846–8851, 2006.
- 699 [42] J. M. Valverde, P. E. Sanchez Jimenez, A. Perejon, and L. A. Perez-Maqueda, “CO<sub>2</sub> multicyclic  
700 capture of pretreated/doped CaO in the Ca – looping process. Theory and experiments,” *Phys.*  
701 *Chem. Chem. Phys.*, vol. 15, pp. 11775 – 11793, 2013.
- 702 [43] J. M. Valverde, “A model on the CaO multicyclic conversion in the Ca-looping process,”  
703 *Chemical Engineering Journal*, vol. 228, pp. 1195–1206, 2013.
- 704 [44] J. Wang, V. Manovic, Y. Wu, and E. J. Anthony, “A study on the activity of CaO-based  
705 sorbents for capturing CO<sub>2</sub> in clean energy processes,” *Applied Energy*, vol. 87, no. 4, pp. 1453  
706 – 1458, 2010.
- 707 [45] A. Martinez, Y. Lara, P. Lisbona, and L. M. Romeo, “Energy penalty reduction in the calcium  
708 looping cycle,” *International Journal of Greenhouse Gas Control*, vol. 7, pp. 74 – 81, 2012.
- 709 [46] P. E. Sanchez-Jimenez, L. A. Perez-Maqueda, and J. M. Valverde, “Nanosilica supported cao:  
710 A regenerable and mechanically hard CO<sub>2</sub> sorbent at Ca-looping conditions,” *Applied Energy*,  
711 vol. 118, pp. 92 – 99, 2014.
- 712 [47] J. M. Valverde, P. E. Sanchez-Jimenez, L. A. Perez-Maqueda, M. Quintanilla, and J. Perez-  
713 Vaquero, “Role of crystal structure on capture by limestone derived CaO subjected to carbon-  
714 ation/recarbonation/calcination cycles at Ca-looping conditions,” *Applied Energy*, vol. 125,



- 715 pp. 264 – 275, 2014.
- 716 [48] P. E. Sanchez-Jimenez, J. M. Valverde, and L. A. Perez-Maqueda, “Multicyclic conversion of  
717 limestone at Ca-looping conditions: The role of solid-state diffusion controlled carbonation,”  
718 *Fuel*, vol. 127, pp. 131 – 140, 2014.
- 719 [49] J. M. Valverde, P. E. Sanchez-Jimenez, and L. A. Perez-Maqueda, “On the relevant influence  
720 of limestone crystallinity on CO<sub>2</sub> capture in the ca-looping technology at realistic calcination  
721 conditions,” *Environmental Science & Technology*, vol. 48, no. 16, pp. 9882–9889, 2014.
- 722 [50] R. A. W. Haul and H. Heystek, “Differential thermal analysis of the dolomite decomposition,”  
723 *American Mineralogist*, vol. 37, no. 3–4, pp. 166–179, 1952.
- 724 [51] P. Caceres and E. Attiogbe, “Thermal decomposition of dolomite and the extraction of its  
725 constituents,” *Minerals Engineering*, vol. 10, no. 10, pp. 1165 – 1176, 1997.
- 726 [52] E. P. Hyatt, I. B. Cutler, and M. E. Wadsworth, “Calcium carbonate decomposition in carbon  
727 dioxide atmosphere,” *Journal of the American Ceramic Society*, vol. 41, no. 2, pp. 70–74, 1958.
- 728 [53] D. Beruto, L. Barco, and A. W. Searcy, “CO<sub>2</sub>-catalyzed surface area and porosity changes in  
729 high-surface-area CaO aggregates,” *Journal of the American Ceramic Society*, vol. 67, no. 7,  
730 pp. 512–516, 1984.
- 731 [54] Y. Wang and W. J. Thomson, “The effects of steam and carbon dioxide on calcite decomposi-  
732 tion using dynamic X-ray diffraction,” *Chemical Engineering Science*, vol. 50, no. 9, pp. 1373  
733 – 1382, 1995.
- 734 [55] J. Khinast, G. Krammer, C. Brunner, and G. Staudinger, “Decomposition of limestone: The  
735 influence of CO<sub>2</sub> and particle size on the reaction rate,” *Chemical Engineering Science*, vol. 51,  
736 no. 4, pp. 623–634, 1996.

- 737 [56] D. Beruto, A. W. Searcy, and M. G. Kim, "Microstructure, kinetic, structure, thermodynamic  
738 analysis for calcite decomposition: free-surface and powder bed experiments," *Thermochimica*  
739 *Acta*, vol. 424, no. 1–2, pp. 99–109, 2004.
- 740 [57] B. Stanmore and P. Gilot, "Review - calcination and carbonation of limestone during thermal  
741 cycling for CO<sub>2</sub> sequestration," *Fuel Processing Technology*, vol. 86, no. 16, pp. 1707–1743,  
742 2005.
- 743 [58] I. Martinez, G. Grasa, R. Murillo, B. Arias, and J. C. Abanades, "Kinetics of calcination  
744 of partially carbonated particles in a Ca-looping system for CO<sub>2</sub> capture," *Energy & Fuels*,  
745 vol. 26, no. 2, pp. 1432–1440, 2012.
- 746 [59] D. Dollimore, J. Dunn, Y. Lee, and B. Penrod, "The decrepitation of dolomite and limestone,"  
747 *Thermochimica Acta*, vol. 237, no. 1, pp. 125–131, 1994.
- 748 [60] M. Samtani, E. Skrzypczak-Janktun, D. Dollimore, and K. Alexander, "Thermal analysis of  
749 ground dolomite, confirmation of results using an X-ray powder diffraction methodology,"  
750 *Thermochimica Acta*, vol. 367–368, pp. 297–309, 2001.
- 751 [61] D. Beruto, R. Vecchiattini, and M. Giordani, "Effect of mixtures of H<sub>2</sub>O (g) and CO<sub>2</sub> (g)  
752 on the thermal half decomposition of dolomite natural stone in high CO<sub>2</sub> pressure regime,"  
753 *Thermochimica Acta*, vol. 404, no. 1–2, pp. 25–33, 2003.
- 754 [62] R. H. Borgwardt, "Calcium oxide sintering in atmospheres containing water and carbon diox-  
755 ide," *Industrial & Engineering Chemistry Research*, vol. 28, no. 4, pp. 493–500, 1989.
- 756 [63] D. Beruto and A. W. Searcy, "Use of the langmuir method for kinetic studies of decomposition  
757 reactions: calcite (CaCO<sub>3</sub>)," *J. Chem. Soc., Faraday Trans. 1*, vol. 70, pp. 2145–2153, 1974.
- 758 [64] S. Dash, M. Kamruddin, P. Ajikumar, A. Tyagi, and B. Raj, "Nanocrystalline and metastable  
759 phase formation in vacuum thermal decomposition of calcium carbonate," *Thermochimica*

- 760 *Acta*, vol. 363, no. 1-2, pp. 129–135, 2000.
- 761 [65] C. Rrodriguez-Navarro, E. Ruiz-Agudo, A. Luque, A. B. Navarro, and M. Ortega-Huertas,  
762 “Thermal decomposition of calcite: Mechanisms of formation and textural evolution of cao  
763 nanocrystals,” *American Mineralogist*, vol. 94, p. 578–593, 2009.
- 764 [66] H.-Y. Xie and D. Geldart, “Fluidization of FCC powders in the bubble-free regime: effect  
765 types of gases and temperature,” *Powder Technol.*, vol. 82, pp. 269 – 277, 1995.
- 766 [67] C. Luo, Y. Zheng, J. Guo, and B. Feng, “Effect of sulfation on CO<sub>2</sub> capture of CaO-based  
767 sorbents during calcium looping cycle,” *Fuel*, vol. 127, pp. 124 – 130, 2014.
- 768 [68] E. O’Neill, D. Keairns, and W. Kittle, “A thermogravimetric study of the sulfation of limestone  
769 and dolomitethe effect of calcination conditions,” *Thermochimica Acta*, vol. 14, no. 12, pp. 209  
770 – 220, 1976.
- 771 [69] N. Ulerich, E. O’Neill, and D. Keairns, “A thermogravimetric study of the effect of pore  
772 volume - pore size distribution on the sulfation of calcined limestone,” *Thermochimica Acta*,  
773 vol. 26, no. 1–3, pp. 269 – 282, 1978.
- 774 [70] J. Agnew, E. Hampartsoumian, J. Jones, and W. Nimmo, “The simultaneous calcination and  
775 sintering of calcium based sorbents under a combustion atmosphere,” *Fuel*, vol. 79, no. 12,  
776 pp. 1515 – 1523, 2000.
- 777 [71] M. E. Diego, B. Arias, G. S. Grasa, and J. C. Abanades, “Design of a novel fluidized bed  
778 reactor to enhance sorbent performance in CO<sub>2</sub> capture systems using CaO,” *Industrial &  
779 Engineering Chemistry Research*, vol. 53, no. 24, p. 10059–10071, 2014.
- 780 [72] R. McCauley and L. Johnson, “Decrepitation and thermal decomposition of dolomite,” *Ther-  
781 mochimica Acta*, vol. 185, no. 2, pp. 271 – 282, 1991.

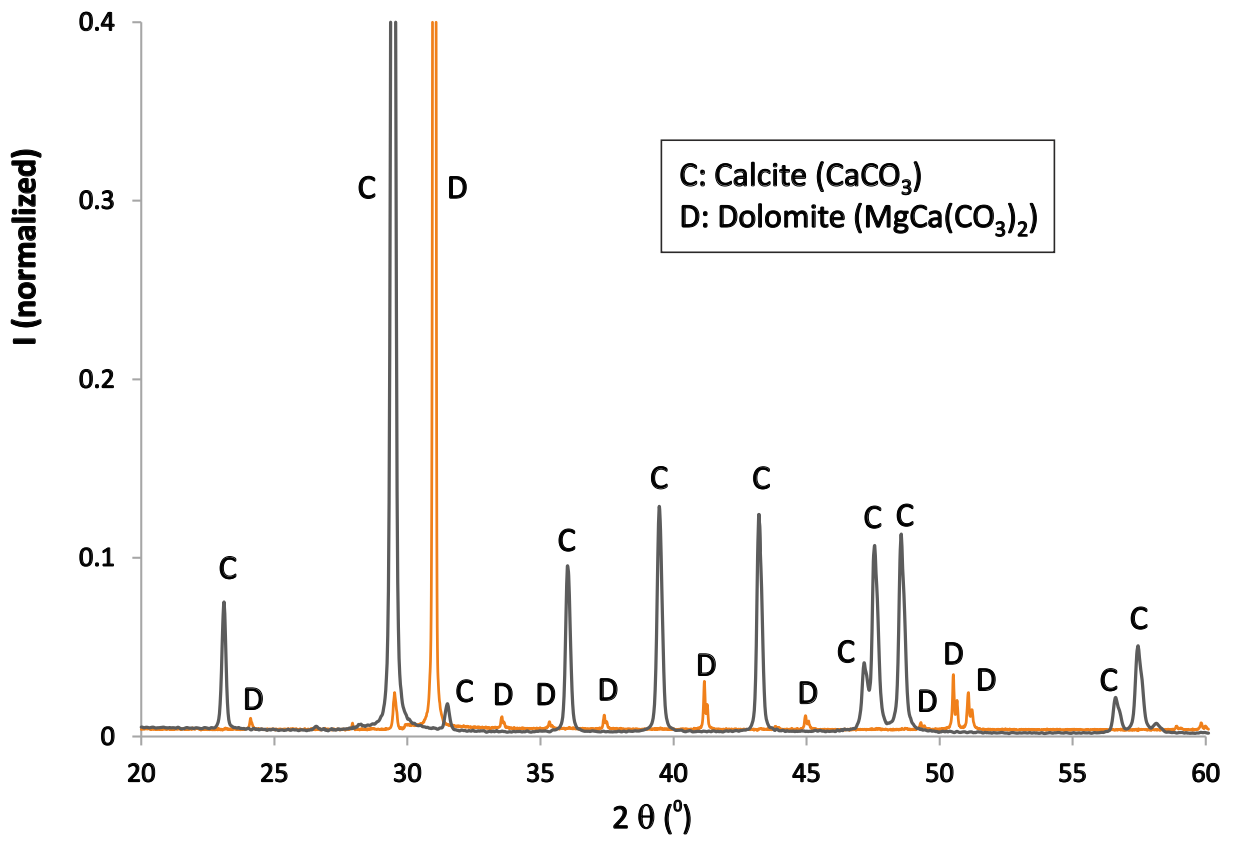


FIG. 1: X-Ray diffractograms measured for samples of dolomite and limestone used in our study (obtained using a Bruker D8 Advance powder diffractometer, Cu-K $\alpha$ ). Values of Intensity are shown normalized to the maximum.

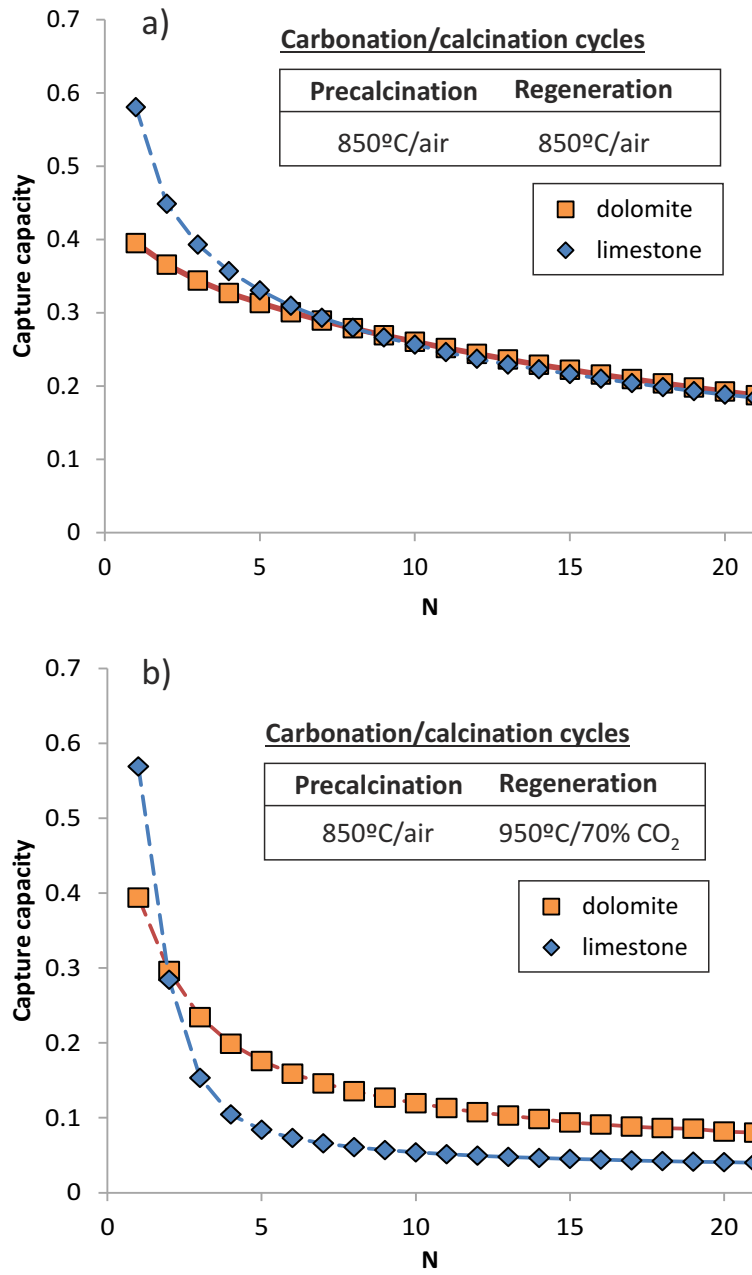


FIG. 2: CO<sub>2</sub> capture capacity as a function of carbonation/calcination cycle number for dolomite and limestone samples precalcined in air and regenerated by calcination either in air at 850°C (a) or under 70%CO<sub>2</sub> at 950°C (b).

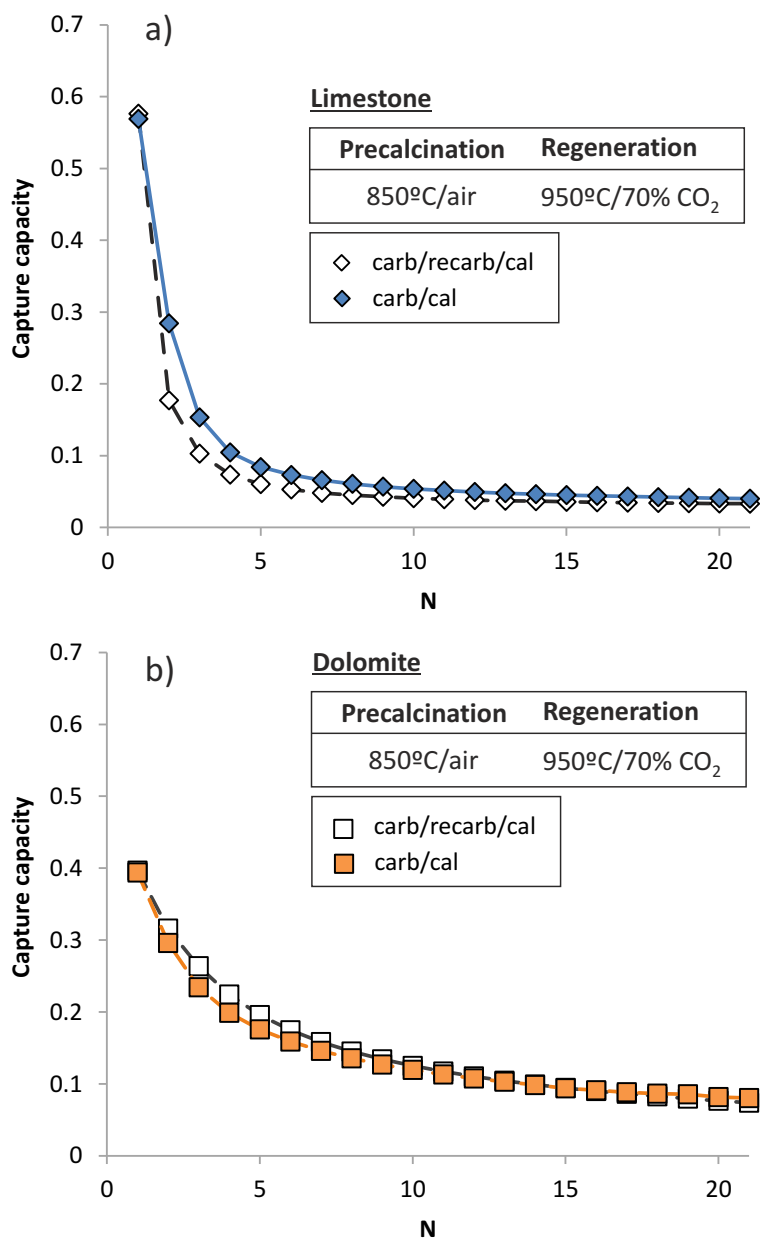


FIG. 3: CO<sub>2</sub> capture capacity as a function of cycle number for limestone (a) and dolomite (b) samples subjected to carbonation/calcination and carbonation/recarbonation/calcination cycles (as indicated), precalcined in air and regenerated by calcination under 70%CO<sub>2</sub> at 950°C.

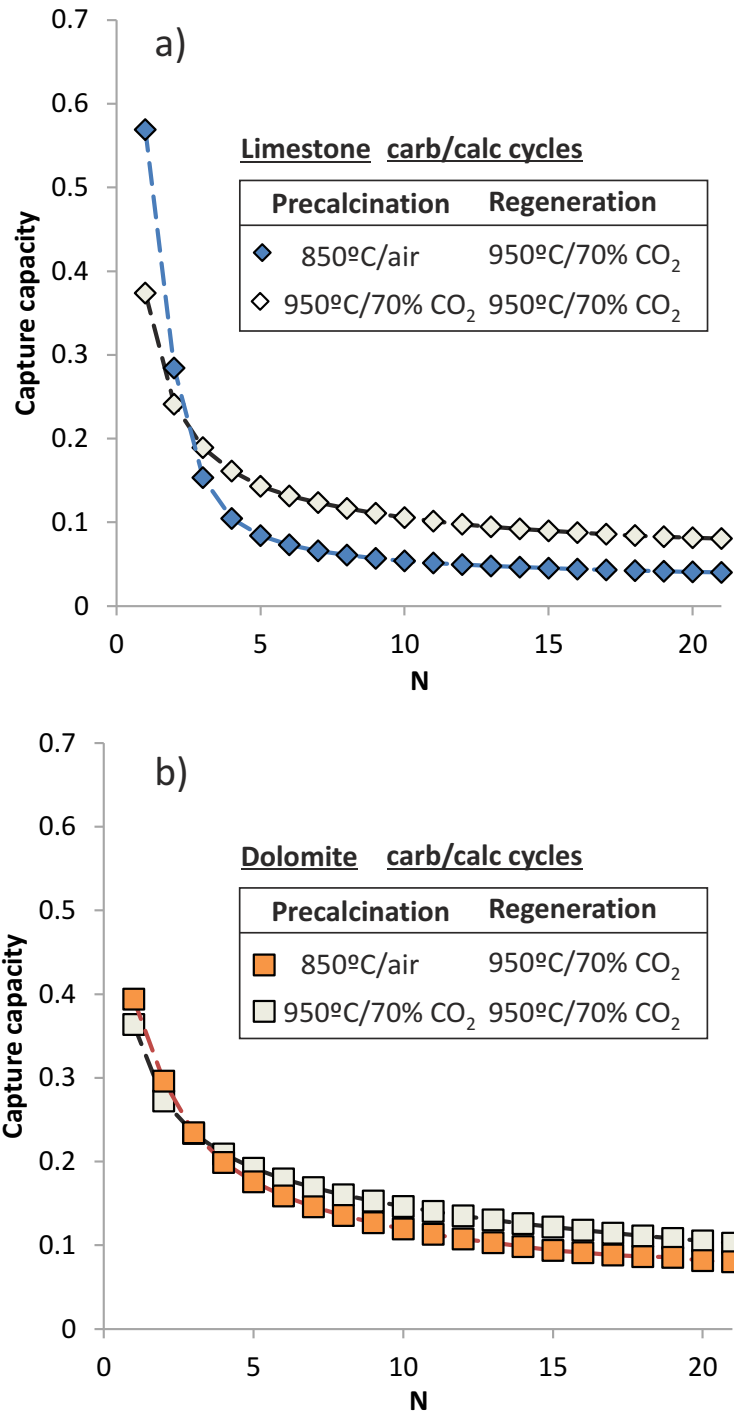


FIG. 4: CO<sub>2</sub> capture capacity as a function of cycle number for limestone (a) and dolomite (b) samples precalcined under different conditions (as indicated) and subjected to carbonation/calcination cycles (regenerated by calcination under 70%CO<sub>2</sub> at 950°C).

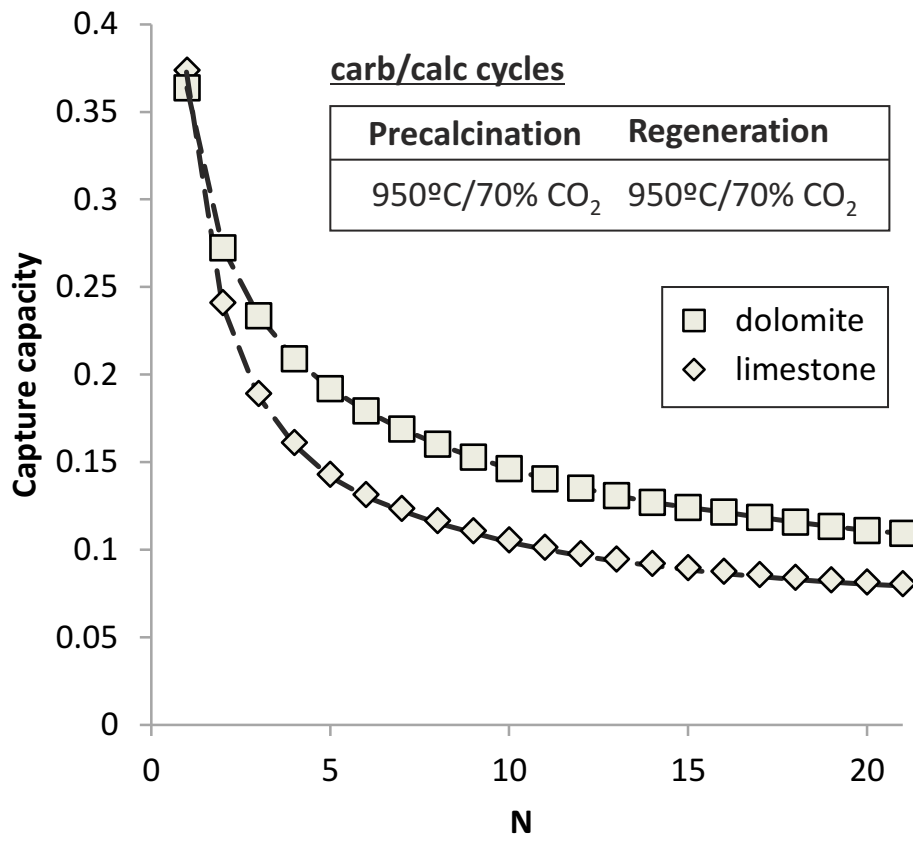


FIG. 5: CO<sub>2</sub> capture capacity as a function of cycle number for limestone and dolomite samples subjected to carbonation/calcination cycles, precalcined and regenerated by calcination under 70%CO<sub>2</sub> at 950°C.



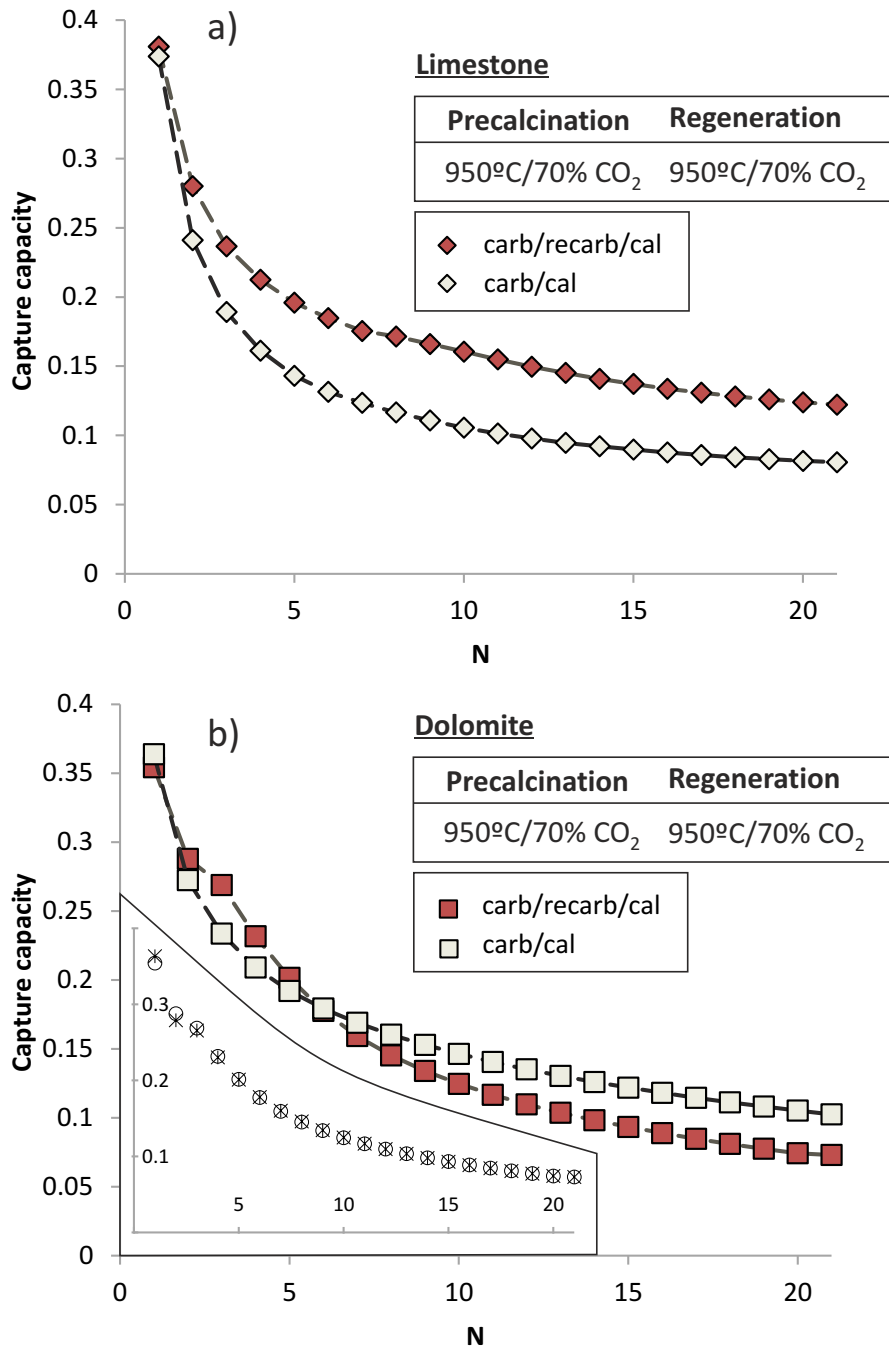


FIG. 6: CO<sub>2</sub> capture capacity as a function of cycle number for limestone (a) and dolomite (b) samples subjected to carbonation/calcination and carbonation/recarbonation/calcination cycles (as indicated) precalcined and regenerated by calcination under 70%CO<sub>2</sub> at 950°C. The inset in b) is a plot of data obtained from tests on different samples of dolomite and same conditions (carb/recarb/calc) to demonstrate results reproducibility.

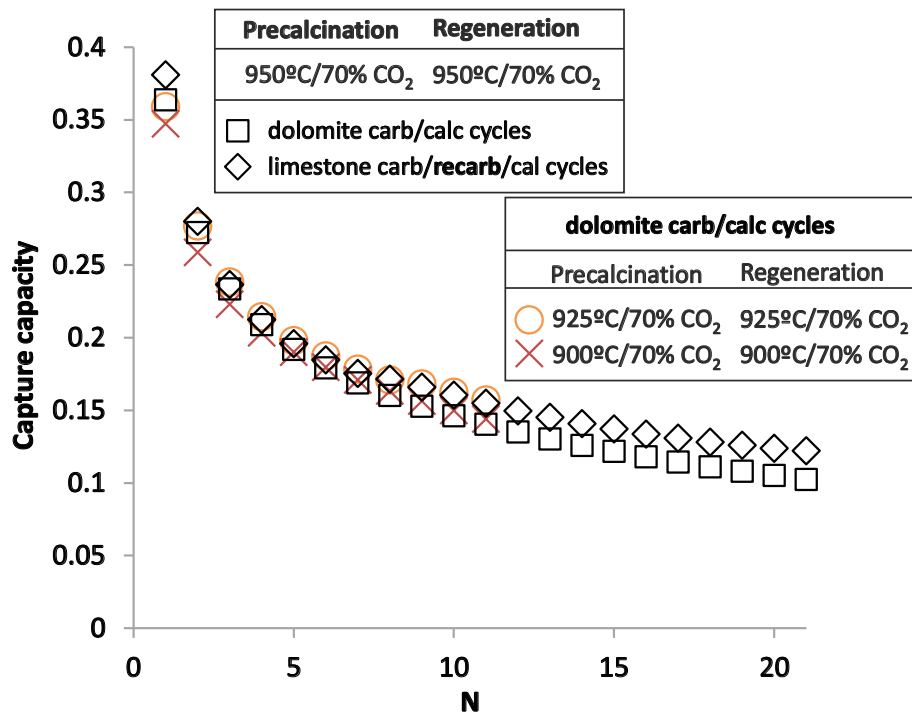
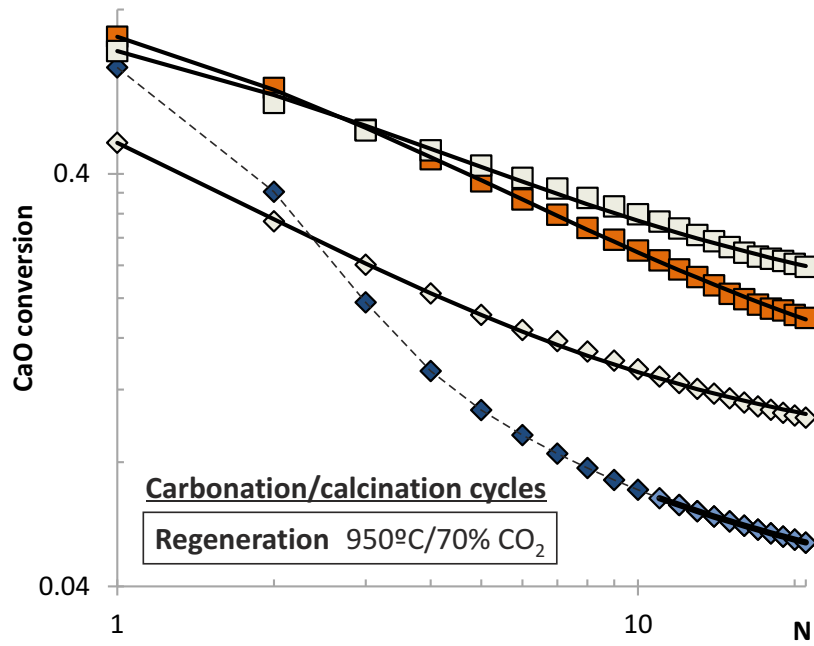


FIG. 7: CO<sub>2</sub> capture capacity as a function of cycle number for dolomite (carbonation/calcination cycles) and limestone samples (carbonation/recarbonation/calcination cycles) precalcined and regenerated by calcination under 70%CO<sub>2</sub> at 950°C.

Results for dolomite samples precalcined and regenerated under 70%CO<sub>2</sub> at 925°C and 900°C are also shown.



Precalcination 950°C/70% CO <sub>2</sub>			Precalcination 850°C/air		
	$k$	$X_r$		$k$	$X_r$
□ dolomite	0.478	0.166	■ dolomite	0.455	0.093
◇ limestone	0.853	0.079	◆ limestone	0.172*	0.034*

FIG. 8: CaO conversion as a function of cycle number (carbonation/calcination cycles) for dolomite and limestone samples regenerated by calcination under 70%CO<sub>2</sub> at 950°C and precalcined as indicated. The solid lines are drawn from the best fits of Eq. 1 to the data. The inset shows the best fitting parameters (deactivation rate  $k$  and residual conversion  $X_r$ ). (\*) In the case of limestone precalcined in air, Eq. 1 fits satisfactorily to the data only from the 10th cycle.

Carbonation/calination cycles    Precalcination 850°C/air    Regeneration 950°C/70% CO<sub>2</sub>

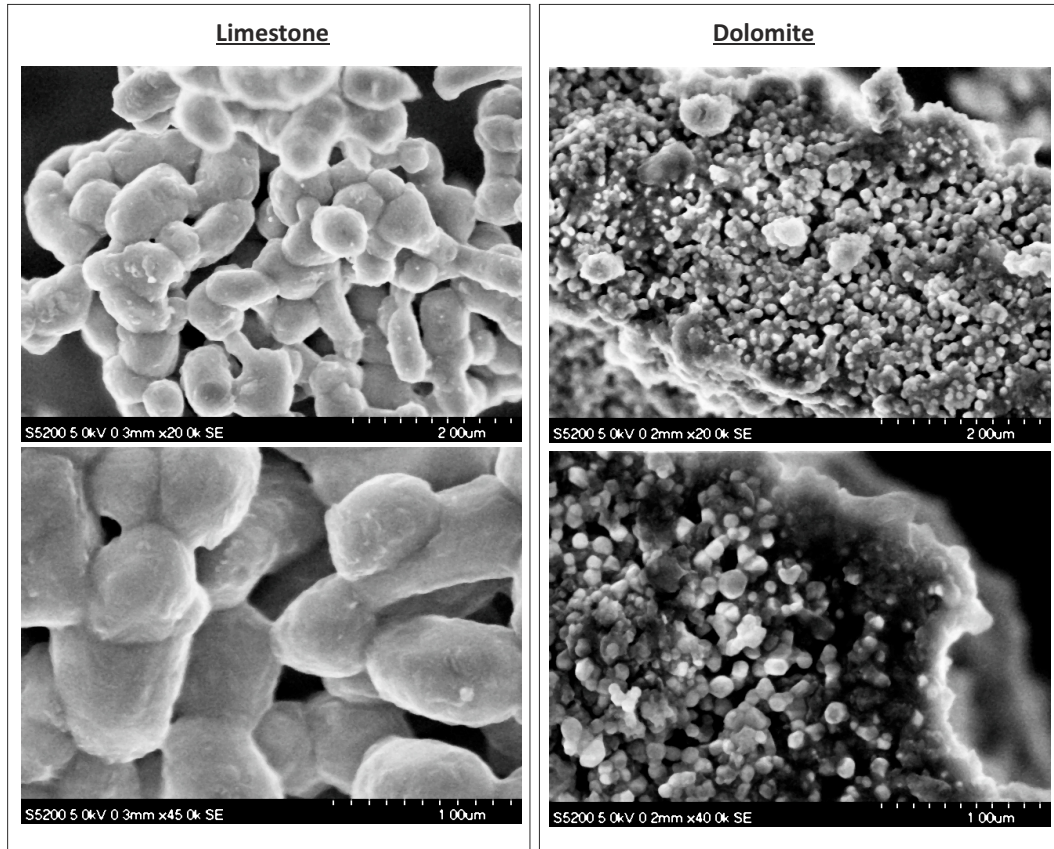


FIG. 9: SEM pictures of limestone and dolomite samples after being subjected to carbonation/calination cycles (precalcined in air (850°C) and regenerated by calcination under 70%CO<sub>2</sub> at 950°C).

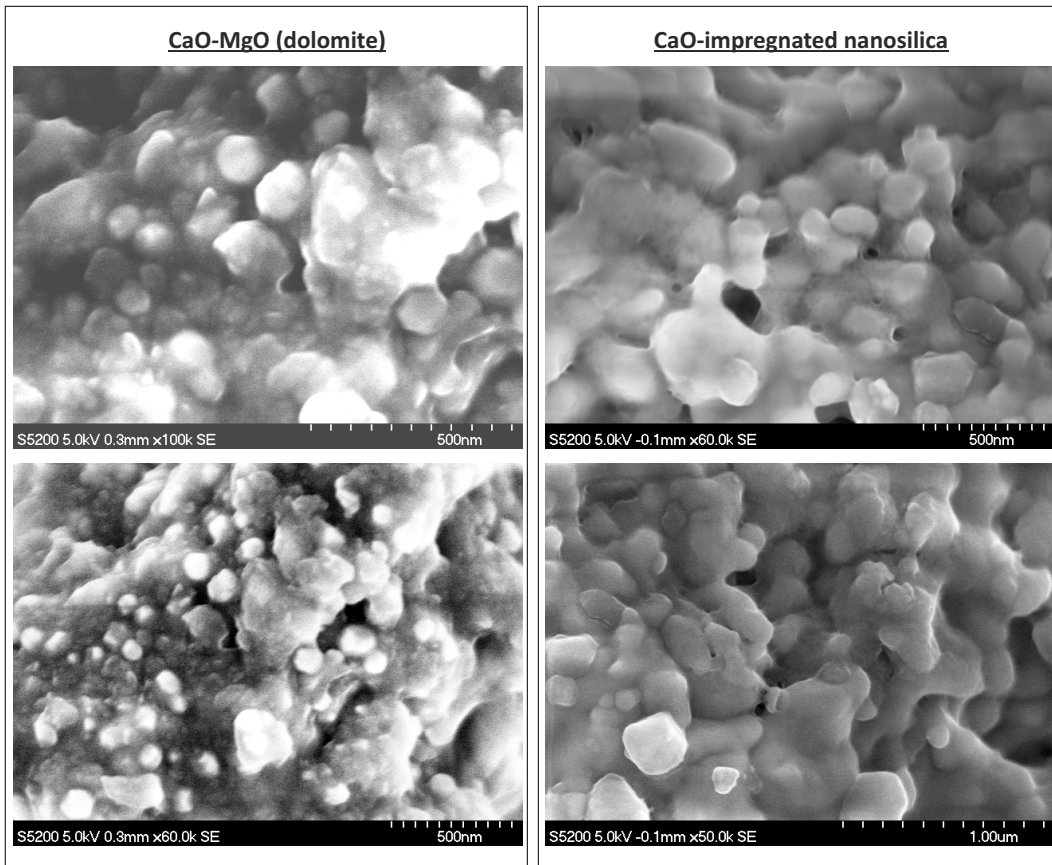


FIG. 10: SEM pictures of: a) dolomite sample after being subjected to carbonation/calcination cycles (regenerated by calcination under 70%CO<sub>2</sub> at 950°C and precalcined in air at 850°C); b) CaO-based sorbent synthesized by impregnation of calcium nitrate solution on a nanostructured calcium silicate matrix after calcination (reported in [46]).

**Carb/recarb/calc cycles Precalcination and regeneration 950°C/70% CO<sub>2</sub>**

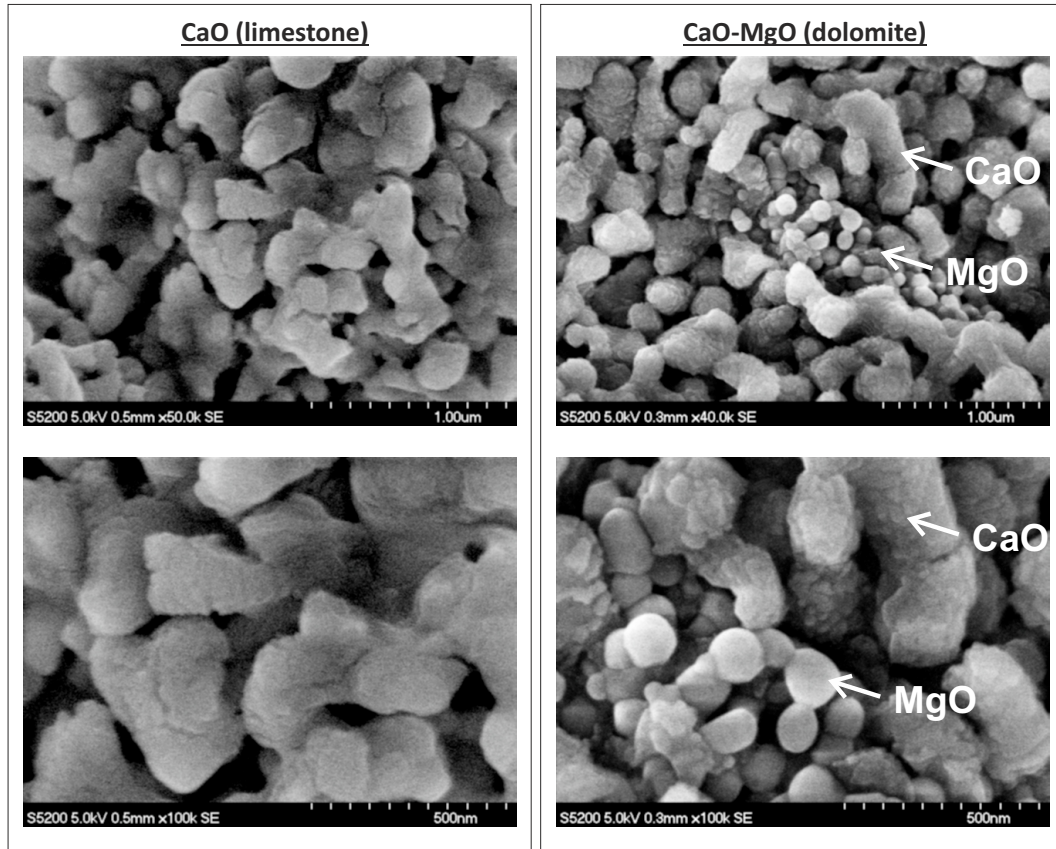


FIG. 11: SEM pictures of limestone and dolomite samples after being subjected to carbonation/recarbonation/calcination cycles (precalcined and regenerated by calcination under 70%CO<sub>2</sub> at 950°C).

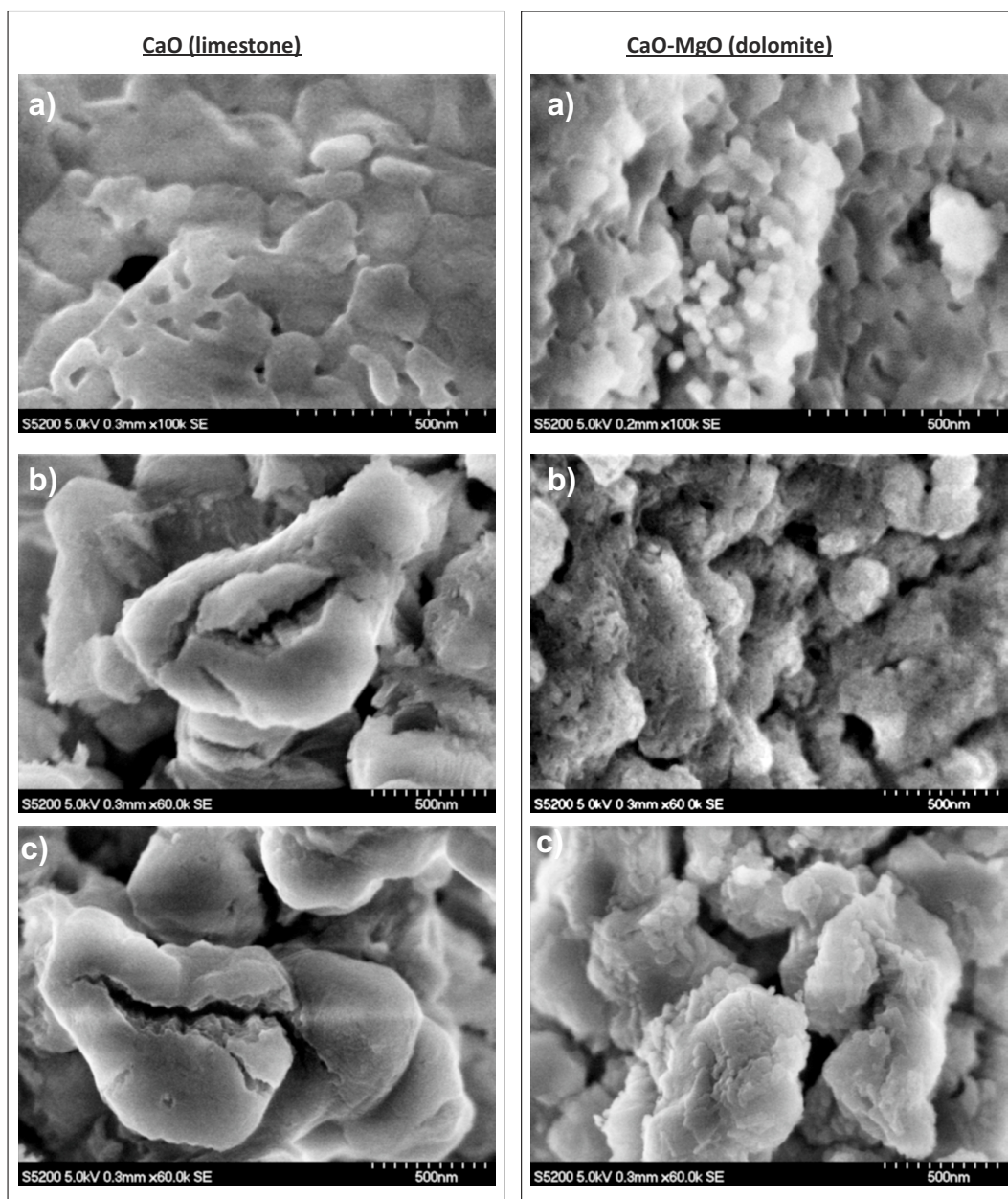


FIG. 12: SEM pictures of limestone and dolomite samples after being cycled under diverse conditions. a) Carbonation/calination cycles (precalcined and regenerated by calcination in air at 850°C). b) Carbonation/recarbonation/calination cycles (precalcined and regenerated by calcination under 70%CO<sub>2</sub> at 950°C). c) Carbonation/calination cycles (precalcined and regenerated by calcination under 70%CO<sub>2</sub> at 950°C).

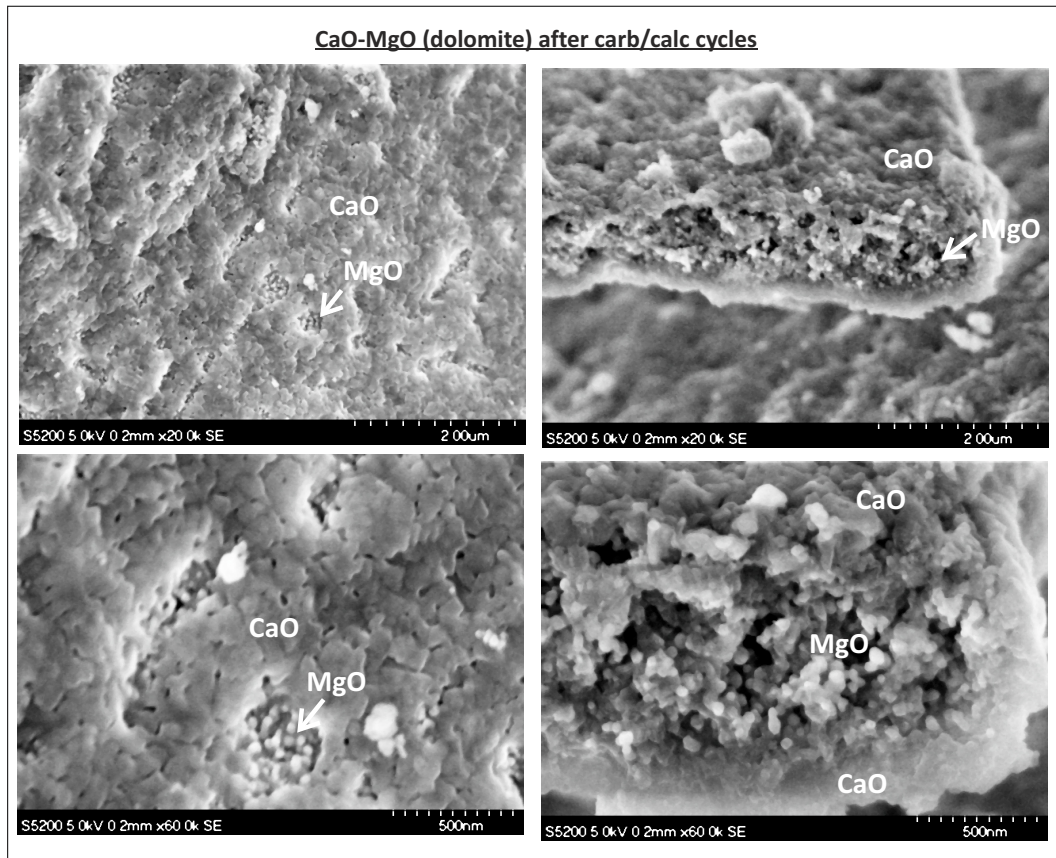


FIG. 13: SEM pictures of a dolomite sample after being subjected to carbonation/calcination cycles (precalcined and regenerated by calcination in air at 850°C).



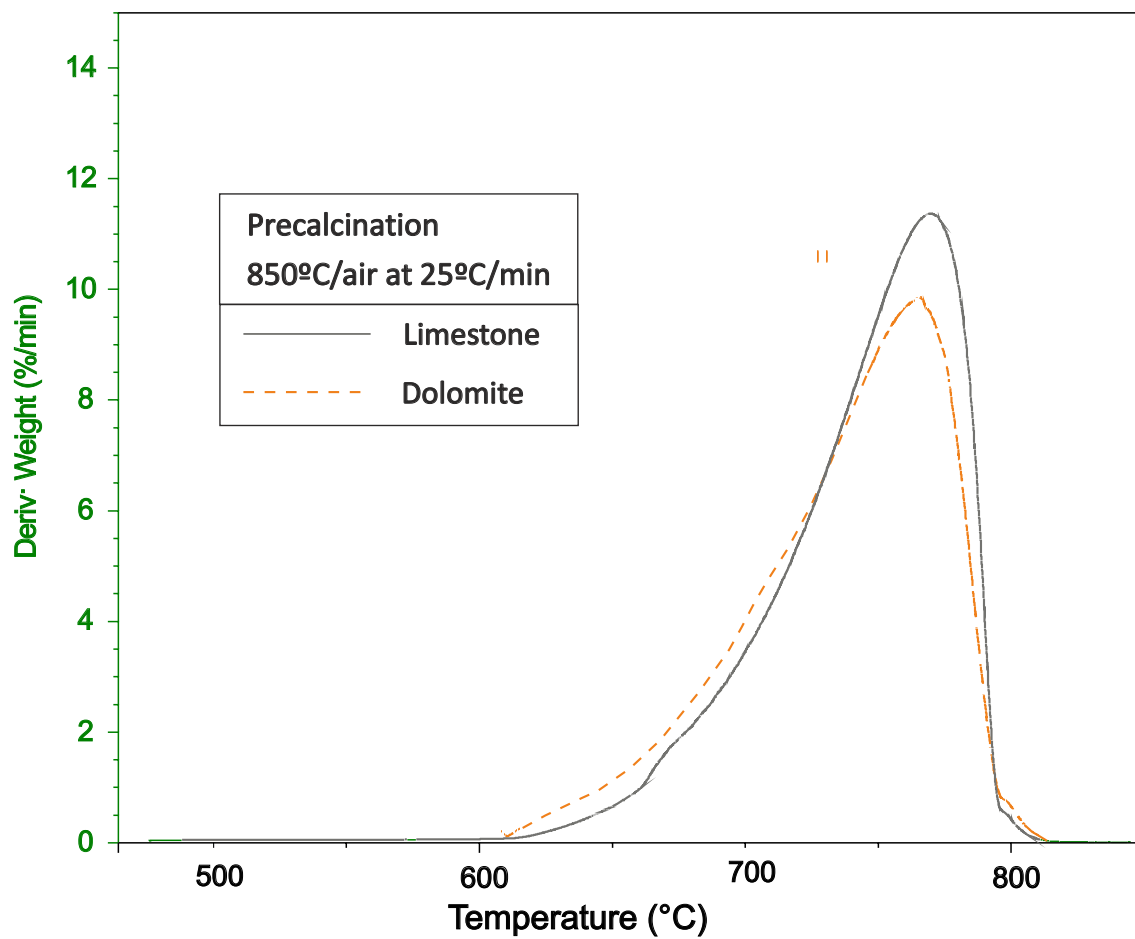


FIG. 14: Derivative of sample weight % (absolute value) as a function of temperature during decomposition of samples of dolomite and limestone precalcined in-situ in the TGA tests under air by slowly increasing the temperature up to 850°C).

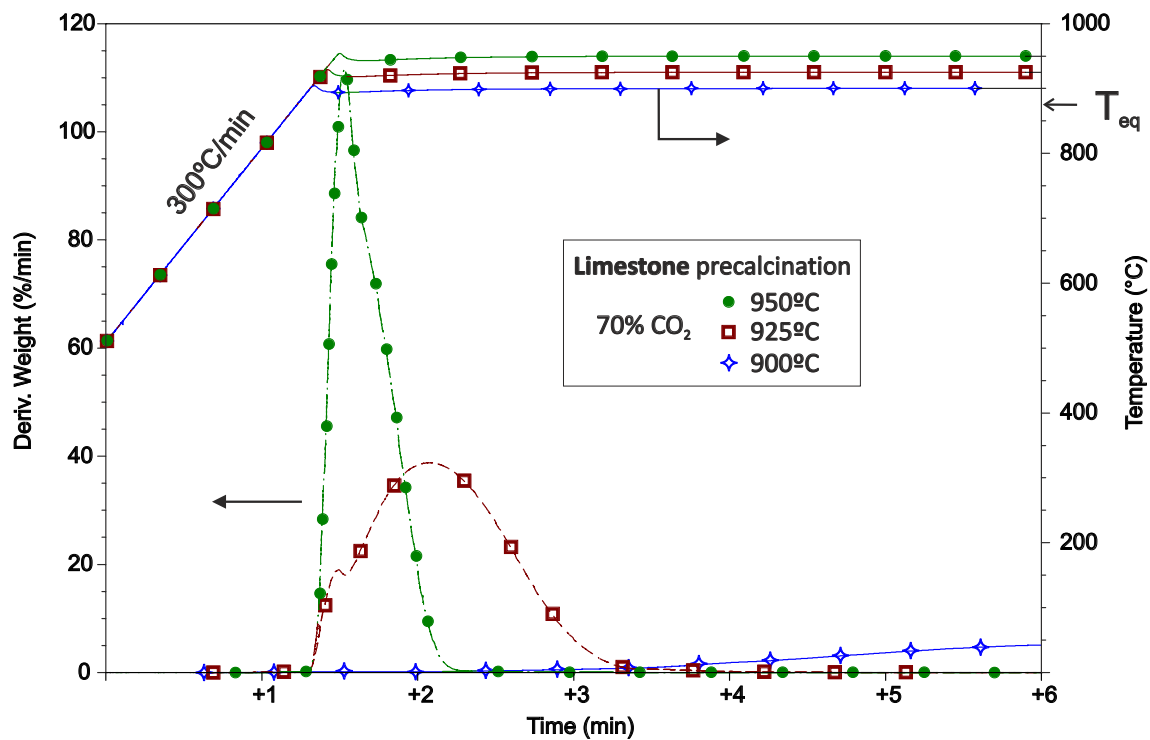


FIG. 15: Time evolution of sample weight % derivative (absolute value) and temperature during decomposition of samples of limestone precalcined in-situ in the TGA tests under 70%CO<sub>2</sub> by quickly increasing the temperature up to 900°C, 925°C, and 950°C (as indicated). The arrow in the temperature axis (right) indicates the thermodynamic equilibrium temperature ( $T_{eq} \approx 870^{\circ}\text{C}$ ).

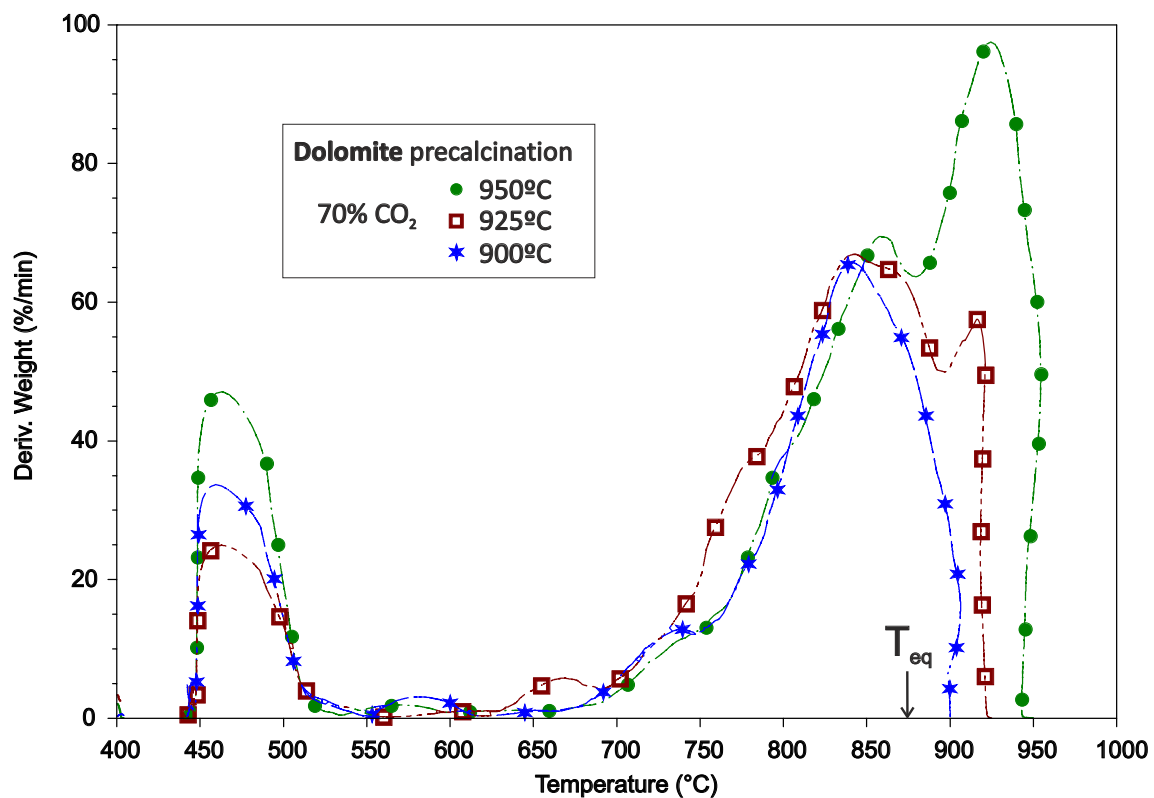


FIG. 16: Derivative of sample weight % (absolute value) as a function of temperature during decomposition of samples of dolomite precalcined under 70%CO<sub>2</sub> in-situ in the TGA tests by quickly increasing the temperature up to 900°C, 925°C, and 950°C ( as indicated). The arrow in the temperature axis (horizontal) indicates the thermodynamic equilibrium temperature for pure calcite ( $T_{eq} \approx 870^\circ\text{C}$ )

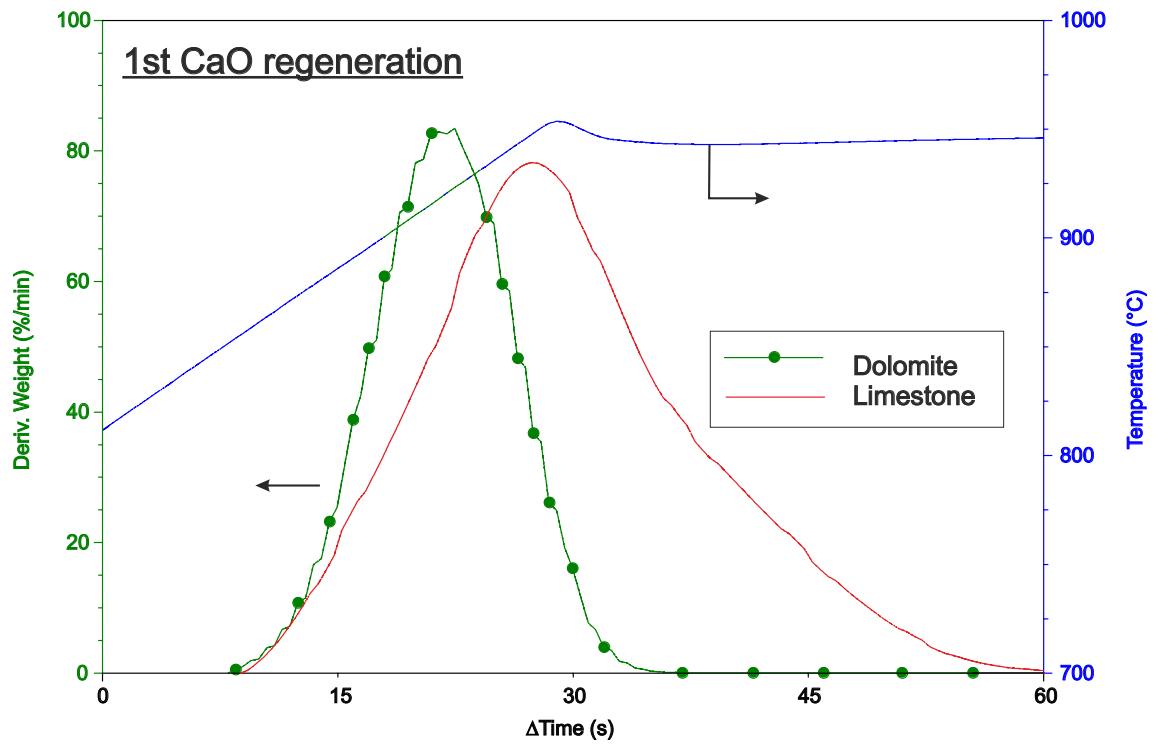


FIG. 17: Time evolution of sample weight % derivative (absolute value) and temperature for samples of limestone and dolomite during 1st regeneration (precalcined and regenerated at 950°C under 70%CO<sub>2</sub>) as indicated).

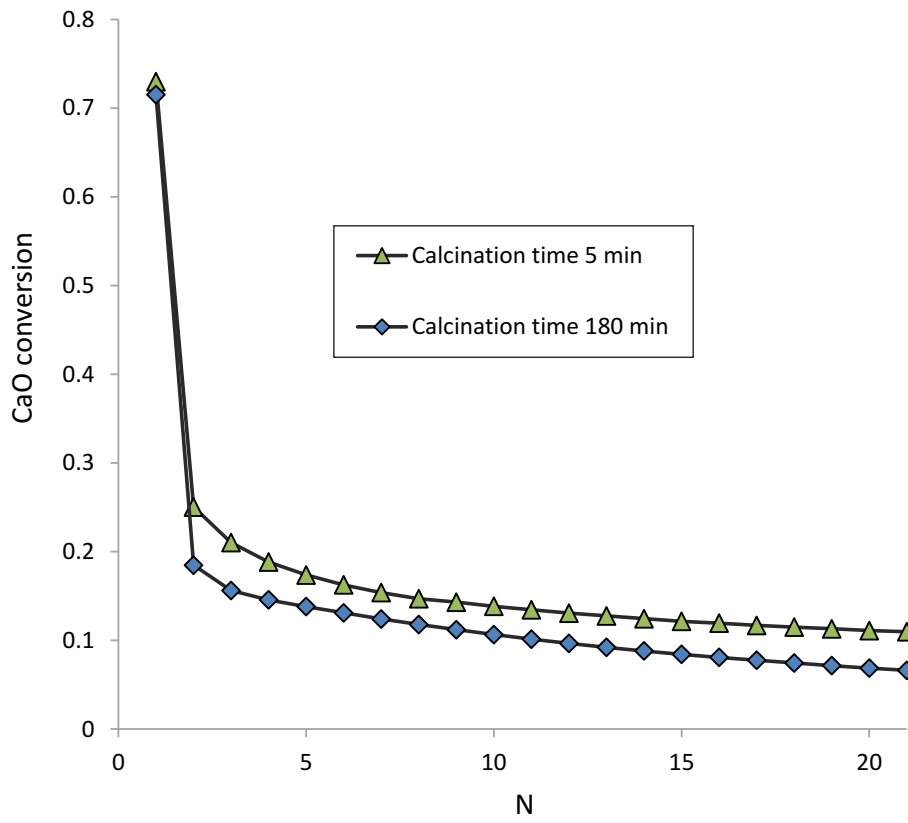


FIG. 18: CaO conversion as a function of cycle number (carbonation/calcination cycles) for limestone samples regenerated by calcination under 70%CO<sub>2</sub> at 925°C (samples precalcined in air at 850°C). Data are shown from tests with different durations of the calcination stages as indicated.